

# Ionisation in atmospheres of brown dwarfs and extrasolar planets

## VI: Properties of large-scale discharge events

R. L. Bailey<sup>1,2</sup>, Ch. Helling<sup>1</sup>, G. Hodosán<sup>1</sup>, C. Bilger<sup>1,3</sup>, C. R. Stark<sup>1</sup>

<sup>1</sup> *SUPA, School of Physics & Astronomy, University of St Andrews, St Andrews, KY16 9SS, UK*

ch@leap2010.eu (July 19, 2022)

<sup>2</sup> *Zentralanstalt für Meteorologie und Geodynamik, Hohe Warte 38, 1190 Vienna, Austria*

<sup>3</sup> *Department of Engineering, University of Cambridge, Cambridge CB2 1PZ, UK*

### ABSTRACT

Mineral clouds in substellar atmospheres play a special role as a catalyst for a variety of charge processes. If clouds are charged, the surrounding environment becomes electrically activated, and ensembles of charged grains are electrically discharging (e.g. by lightning), which significantly influences the local chemistry creating conditions similar to those thought responsible for life in early planetary atmospheres. We note that such lightning discharges contribute also to the ionisation state of the atmosphere. We apply scaling laws for electrical discharge processes from laboratory measurements and numerical experiments to DRIFT-PHOENIX model atmosphere results to model the discharge's propagation downwards (as lightning) and upwards (as sprites) through the atmospheric clouds. We evaluate the spatial extent and energetics of lightning discharges. The atmospheric volume affected (e.g. by increase of temperature or electron number) is larger in a brown dwarf atmosphere ( $10^8 - 10^{10} \text{ m}^3$ ) than in a giant gas planet's ( $10^4 - 10^6 \text{ m}^3$ ). Our results suggest that the total dissipated energy in one event is  $< 10^{12} \text{ J}$  for all models of initial solar metallicity. First attempts to show the influence of lightning on the local gas phase indicate an increase of small carbohydrate molecules like CH and CH<sub>2</sub> at the expense of CO and CH<sub>4</sub>. Dust forming molecules are destroyed and the cloud particle properties are frozen-in unless enough time is available for complete evaporation. We summarise instruments potentially suitable to observe lightning on extrasolar objects.

*Subject headings:* brown dwarfs, atmospheres, dust, ionisation, magnetic coupling

## 1. Introduction

Atmospheric electrical discharges are observed within our solar system (e.g. Desch 1992; Zarka et al. 2008; Dyudina et al. 2004; Fischer et al. 2011), most notably Earth, where lightning is a common large-scale discharge phenomenon. There are lesser-known discharges of even larger scales that occur in Earth’s upper atmosphere such as blue jets and giant red sprites, a fraction of which is triggered by a lightning strike (e.g. Boccippio et al. 1995).

Discharges within the atmospheres of Jupiter and Saturn have also been detected (e.g. Rinnert et al. 1998; Little et al. 1999; Dyudina et al. 2004; Fischer et al. 2011); Jupiter’s discharges have been observed and imaged in the optical and corresponding radio emissions have also been detected. Saturn is very loud in the radio, giving off bursts of SEDs (Saturn Electrostatic Discharges) when a discharge (lightning) storm develops in its atmosphere. Both of these planets have estimated total discharge energies of  $\approx 10^{12} - 10^{13}$  J, much larger than the values of  $10^8 - 10^9$  J of a single lightning strike energy on Earth. Observable discharges on these giant gas planets appear less common and are more localised compared to Earth. Electromagnetic signatures from discharges in the atmospheres of Uranus and Neptune have also been detected (Gurnett et al. 1990; Zarka & Pedersen 1986); however, these measurements are sparse and little is known about the properties of discharges on the outermost gas planets.

Electrostatic discharges have long been thought to be a catalyst for the creation of prebiotic molecules responsible for the origin of life on the young Earth (Miller & Urey 1953), and so the scales of discharges and the amount of energy deposited into an exoplanetary atmosphere are of great interest. Also of interest is whether the discharge events are large and/or strong enough to be detectable from afar, as the presence of detectable emissions could reveal information on the local physicochemical processes and the chemical composition within other atmospheres. In this paper we present the first study of the characteristic scales of lightning discharges in very cool, low mass objects.

Zarka et al. (2012) estimate that it is not totally unrealistic to detect lightning on a extrasolar gas giant planet at a distance of 10pc. It would need to have lightning discharges emitting  $10^5 \times$  more energy than Jupiter. Brown dwarfs are of Jupiter’s size and a large fraction are more active than Jupiter due to their fast rotation which drives atmospheric circulation and cloud formation processes. While Earth’s cloud lightning storms are dispersed across the planet, Jupiter’s discharges are observed to only occur within certain storm cells. Saturn’s SEDs seem to be observable when a single massive storm (some large enough to contain many Earths) forms within its atmosphere.

We may argue that indications for lighting, or the electromagnetic signature of high-

energy discharge processes, may have already been detected in extrasolar substellar atmospheres. While quiescent X-ray emission decays between objects of spectral class M7 and M9 (Berger et al. 2010), objects as cool as L5/T7 brown dwarfs exhibit long-lived  $H\alpha$  emission and quiescent radio emission (Hall 2002; Burgasser et al. 2011, 2013). Route & Wolszczan (2013) and Williams et al. (2013a) observed the radio emission from a T6.5 dwarf. The physical mechanism behind flaring, quiescent X-ray and radio emission may be the result of the energy release into the ambient atmosphere associated with reconnecting magnetic field lines. This implies a coupling between the bulk, convective motions of the atmosphere and the ambient magnetic field. Despite uncertainty regarding the origin of magnetic fields in fully convective objects, the more pressing question is which processes contribute to the ionisation of such ultra-cool atmospheres such that convective energy can be released by magnetic field coupling. This paper will contribute to resolving this question by presenting a first study of large-scale discharge properties in extrasolar, ultra-cool atmospheres.

Other plasma-initiated emission may also be present in substellar atmospheres. Magnetospheric electrons that are accelerated along magnetic field lines will interact with the neutral atmosphere stimulating auroral-type emission as suggested in Nichols et al. (2012). However, a seed plasma is also required for such auroral emissions which originate from the solar wind, cosmic rays and the geologically active Io in the Jupiter system. It might be suggestive to think about moons in conjunction with satellite systems (that exert tidal forces on the moon) as plasma sources for exoplanets, similar sources (incl. host star winds) can not a priori be expected to be available to brown dwarfs or brown dwarf systems. Hence the same question arises, namely, where does the seed plasma come from that drives an aurora.

The onset of lightning is not well understood (e.g. MacGorman & Rust 1998). However, streamer discharges are thought to play a major role and are suggested to determine the early stages of large-scale discharges like lightning and associated sprites (Phelps 1974; Raizer 1991; MacGorman & Rust 1998; Briels et al. 2008a) as they occur in a variety of ionised media with a large range of pressure and temperature.

We adopt the idea that a large-scale lightning strike or a large-scale sprite discharge is composed of various small streamer events, and that a streamer triggers and develops into such a large-scale discharge event. This is not always the case since most of the gas-discharges in an atmosphere may in fact not even develop into a streamer (see e.g. Helling et al. 2013). However, in this paper we are interested in investigating the scales that large-scale gas-discharges can develop, what atmospheric volume might be affected, and what amount of energy may be deposited into the atmospheres of brown dwarfs and planets by large-scale lightning discharges. We also discuss how the local gas phase can be affected by the temperature increase in a discharge channel in the atmosphere.

We utilised scaling laws for discharge processes based on laboratory measurements (Briels et al. 2008a,b; Nijdam et al. 2008) and numerical experiments (Pancheshnyi et al. 2005) in order to provide a first investigation of the spatial extent and energetics of discharges within the atmospheres of substellar objects, i.e. in brown dwarfs and extrasolar giant gas planets. In principle, these investigations can also be applied to smaller planets such as those currently observed by the *Kepler* space mission.

We start with a summary (Sect. 2) of our work on clouds in the atmospheres of brown dwarfs and giant gas planets. Section 3 introduces the scaling laws which we use and outlines our method of applying these scaling laws to brown dwarf and giant gas planet atmospheres. Section 4 summarises our results. Lightning on Earth produces a large number of observable signatures accross the energy spectrum. We summerise these signatures in Sect. 7 and collate possible instruments for their detection on Brown Dwarfs or exoplanets.

## 2. Cloudy Substellar Atmospheres

Atmospheres of very cool, substellar objects like brown dwarfs (BD) and giant gas planets (GP) are cold and dense enough that cloud particles can condense from the atmospheric gas. The formation of dust by seed formation and bulk growth takes place in a temperature window of  $\approx 500 - 2100$  K and leads to the formation of mineral clouds. Gravitational settling, convective mixing and element depletion are major processes that occur in such atmospheres. Helling, Woitke & Thi (2008) have shown that the upper cloud region (low-temperature and low-pressure) will be dominated by small, dirty (i.e. inclusions of other materials) silicate grains with inclusions of iron and metal oxides; and the warmer, denser cloud base by bigger, dirty iron grains with metal inclusions. The actual size of the cloud particles deviate from this mean value according to a height dependent size distribution (Fig. 8 in Helling, Woitke & Thi 2008). The chemical material compositions as well as the local grain size distribution change with height inside a cloud in a quasi-stationary environment. These cloud particles can be charged (Helling et al. 2011a) and the resulting electric field may be sufficiently strong to initiate small-scale streamers that develop into large-scale discharge processes like lightning (Helling et al. (2011b, 2013)).

We utilise one-dimensional atmosphere models in what follows, hence, we do not take into account any horizontal motions that are so obvious on Jupiter and are stipulated for irradiated, extrasolar planets from works by Showman et al. (e.g. Showman et al. 2013a). Such horizontal motions will produce patchy cloud coverage rather than a homogeneous cloud coverage as assumed in 1D models. More complicated atmospheric structures involving winds and dynamic meteorology will introduce additional effects such as ionization via Alfvén

ionization (Stark et al. 2013).

## 2.1. Atmospheres and Clouds

We use DRIFT-PHOENIX model atmosphere structures (Dehn 2007; Helling et al. 2008a,b; Witte et al. 2009, 2011) as input for the local gas temperature and gas pressure. DRIFT-PHOENIX model atmospheres are determined by a coupled system of equations describing radiative transfer, convective energy transport (modelled by mixing length theory), chemical equilibrium (modelled by laws of mass action), hydrostatic equilibrium and dust cloud formation. The dust cloud formation model includes a model for seed formation (nucleation), surface growth, evaporation of mixed materials and gravitational settling (Woitke & Helling 2003, 2004; Helling & Woitke 2006; Helling, Woitke & Thi 2008; Helling & Fomins 2013). The results of the DRIFT-PHOENIX model atmosphere simulations include the gas temperature - gas pressure structure ( $T_{\text{gas}}, p_{\text{gas}}$ ), the local gas-phase composition, the local electron number density ( $n_e$ ), the number of dust grains ( $n_d$ ) and their mean sizes ( $\langle a \rangle$ ); which are all dependent on atmospheric height. These models are determined by the effective temperature,  $T_{\text{eff}}$ , the surface gravity,  $\log(g)$ , and the initial element abundances which are set to solar values unless specified otherwise.

Atmospheres of varying parameters were used: The effective temperatures, which represent the total wavelength-integrated radiative flux, ranged from 1500 K to 2000 K. Within each effective temperature category, the substellar atmospheres split into categories of brown dwarfs (BDs;  $\log(g) > 4.0$ ) and giant gas planets (GPs,  $\log(g) < 4.0$ ), for which we consider solar metallicity ( $[M/H] = 0.0$ ) and sub-solar metallicity ( $[M/H] = -3.0$ ) models. The initial element abundances are oxygen-rich, i.e. more oxygen than carbon is available.

Dusty cloud layers are expected to form within these substellar atmospheres. With the formation of initial seed particles, chemicals can gather on their surface and dust grains grow while simultaneously depleting the local elemental abundances. As the grains grow in mass, they fall down through the cloud and gravitationally settle in the lower layers. Convection in the atmosphere allows for the constant replenishment of chemicals in the cloud for the growth of dust grains, as well as the mixing of dust grains of different size and composition (Helling et al. 2008c).

Due to the 1D nature of the models, the clouds are assumed to form in horizontally extended layers within the atmospheres. The cloud deck is here defined as the first particle nucleation maximum and the point at which all cloud particles have evaporated due to the

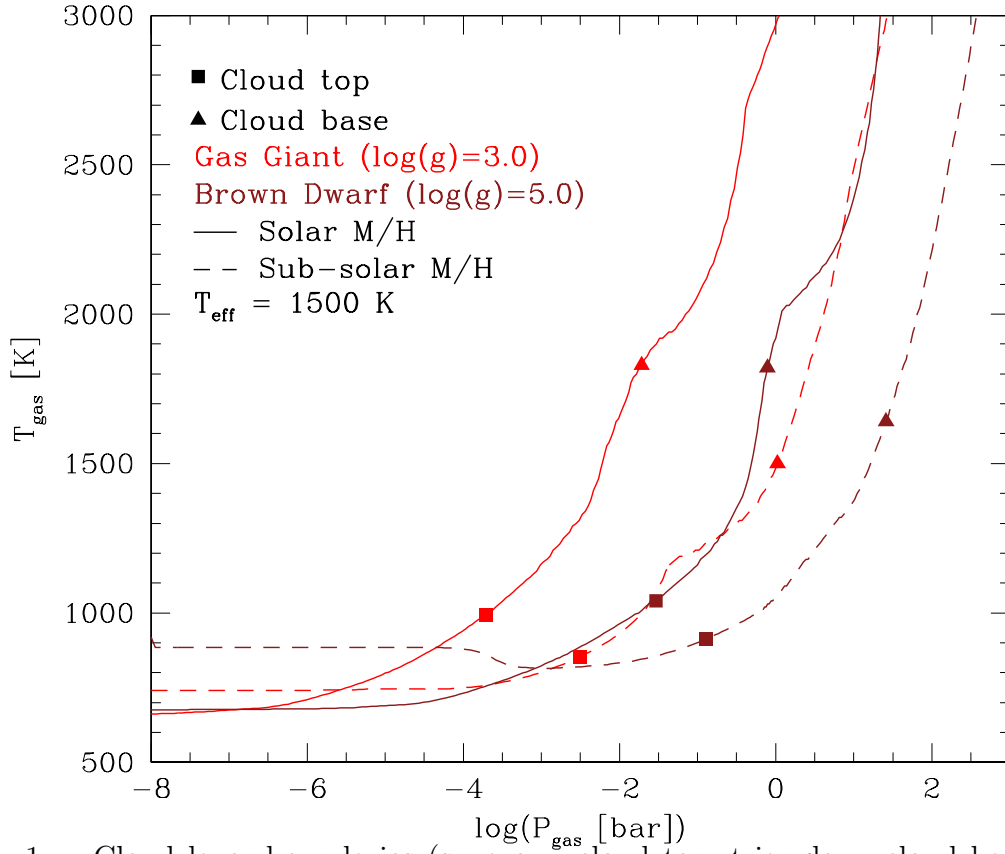


Fig. 1.— Cloud layer boundaries (square = cloud top, triangle = cloud base) in DRIFT-PHOENIX model atmosphere structure of brown dwarfs (brown) and giant gas planets (red) with  $T_{\text{eff}} = 1500 \text{ K}$ . Over-plotted are two cases of different metallicity (solar,  $[M/H] = 0.0$  – solid lines; sub-solar,  $[M/H] = -3.0$  – dashed lines).

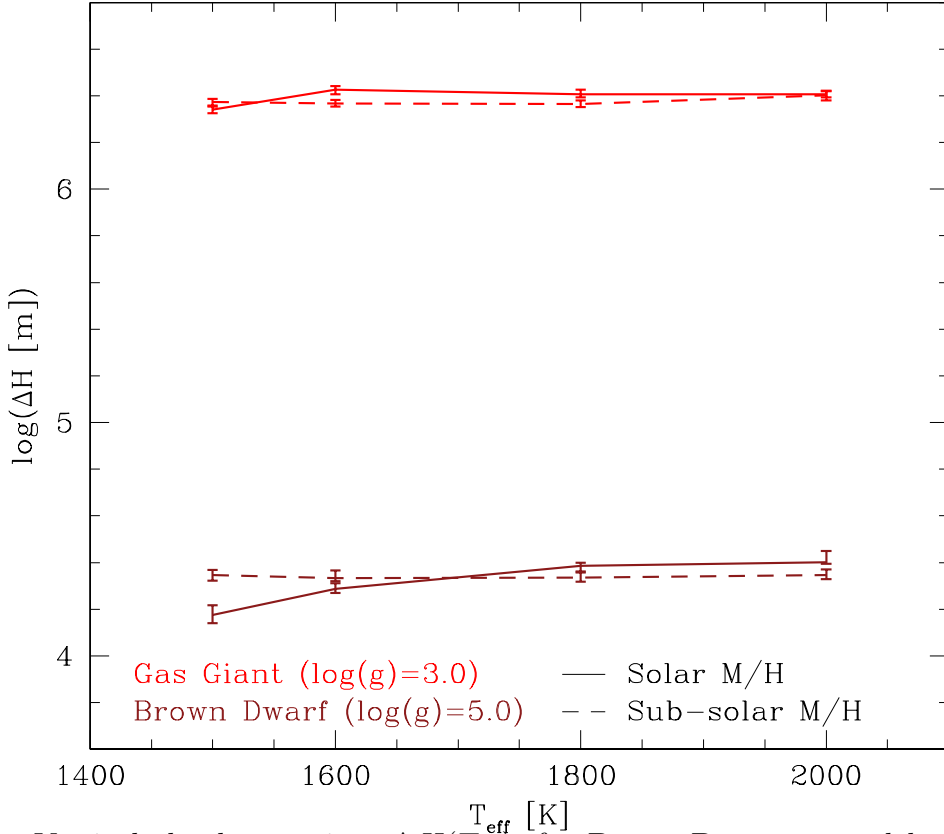


Fig. 2.— Vertical cloud extension,  $\Delta H(T_{\text{eff}})$ , for DRIFT-PHOENIX model atmospheres of different  $T_{\text{eff}}$  with  $\log(g) = 3.0$  (GP, red),  $5.0$  (BD, brown);  $[M/H] = 0.0$  (solid lines),  $-3.0$  (dashed lines). The error bars indicate the uncertainty with which the cloud height is determined based on the DRIFT-PHOENIX atmosphere models (see also Sect 5.2).

locally high temperature<sup>1</sup>. These cloud decks are usually of the order of  $10^7$  m in vertical extension ( $\Delta H$ ) in the GPs and  $10^4$  m in the BDs due to the higher surface gravity (Fig. 2). Clouds in low-metallicity atmospheres form at lower temperatures and higher pressures than clouds in the solar-metallicity atmospheres (Witte et al. 2009). GP atmospheres also form clouds at much lower pressures than their BD counterparts (Fig. 1). With increasing effective temperature, the clouds also form at decreasing pressure, hence they are located at higher atmospheric altitudes.

## 2.2. Large-scale charge separation within clouds

Charge separation requires motion and friction for the separation and relocation of charges to occur. This can be provided by convective and turbulent motions, which are common in atmospheres and cloud regions, and have been observed in the cloud and storm systems of Jupiter and Saturn. Large-scale motions (global circulation patterns) on exoplanets are inferred from thermal emission observations from infrared lightcurves e.g. (Knutson et al. 2012) and from simulations e.g. (Heng et al. 2011; Dobbs-Dixon et al. 2012; Rauscher & Menou 2012; Perna et al. 2012; Showman et al. 2013b). All suggest a displacement of the hot-spot (a global temperature maximum of the atmosphere due to irradiation by the host star) as result of a fast eastward windflow at the equator that displaces the thermal maxima to the east. Resulting differential, height-dependent rotation of the atmosphere can naturally be expected. Collisions between the cloud particles can lead to tribo-electric charging, which occurs due to friction as one material surface rubs against another and charge is transported from one grain to another. Experiments show that in systems of colliding particles, negative charge moves to the smaller particles while the larger particles become positively charged (Lacks and Levandovsky, 2007; Krauss et al., 2003; Zheng et al., 2003). Larger particles will sink faster to the bottom of the cloud while smaller particles remain longer at the top and can be easily transported by winds, establishing large-scale charge separation within the cloud. Similar scenarios are suggested in Merrison et al. (2012); Zarka et al. (2004), and in Farrell et al. (1999).

Another mechanism at work in very turbulent atmospheres would be fracto-emission. Fracto-emission is the emission of particles and electrons during and after the fracture of a dust grain due to external stresses. This process results in the emitted, fractured material acquiring different charges (Dickinson et al. 1984). The different transport properties of the charged grains cause them to migrate within the dust cloud and an electric field can be

---

<sup>1</sup>See Eq. 16 in Woitke & Helling (2004) for a different definition of the cloud height.

established. The shattering process depends strongly on the relative velocities involved in the collisions.

### 3. Application of gas-discharge scaling laws to brown dwarf and giant gas planetary atmospheres

We aim to investigate the geometrical extension of potential discharge processes in BD and GP atmospheres, and to find out where potential lightning discharges occur. We utilise experimentally obtained scaling laws (*similarity relations*) describing discharge properties to provide a first insight into the potential scale size of discharge processes in BDs and GPs and derive values for the energy deposited and the atmospheric volume affected. Knowing both the pressure-temperature scales in our model atmospheres and the cloud extensions (from DRIFT-PHOENIX atmosphere simulations) enables us to estimate how discharge properties (such as the discharge propagation length, the radius of the discharge channel or the gas volume affected by the discharge) scale within the modelled cloud layers.

We first outline our modelling ansatz in Sects. 3.1– 3.3. Section 3.4 introduces the scaling laws which we utilise.

#### 3.1. Modelling ansatz

To investigate atmospheric discharge events we model the top and bottom of the cloud layer as two equal and oppositely charged surfaces analogous to the parallel plates of a capacitor. This ansatz has been applied by Raizer et al. (1998), Yair et al. (2009) and by Pasko et al. (2000) to study sprites in solar system planetary atmospheres and fractal streamer propagation. It serves as a first-order-approximation to investigate the latent physics and chemistry of the system. It is assumed that a streamer-initiated discharge can occur between two charge-carrying surfaces (i.e. the cloud top and the cloud base) if the build-up of electric charge is large enough for the resulting electric field to overcome the local breakdown field.

The net charge on the cloud top and base (and hence the resulting electric field) is unknown, unless all necessary charging processes can be modelled. Therefore, a two-fold strategy was followed to evaluate the electric field which was inspired by previous works (Raizer et al. (1998); Pasko et al. (2000); Yair et al. (2009)).

In case (i)  $Q = \text{const}$ : the local electric field is evaluated by assuming a constant charge  $Q$ . The discharge would then propagate from a point in the cloud,  $z_{\text{init}}$  at which the local electric field  $E(z_{\text{init}}, Q)$  corresponding to charge  $Q$ , exceeds the break-down field strength

$E_{\text{th}}$ :  $E(z, Q) > E_{\text{th}}$ . The exact position of this point and the distance from the cloud top varies between the different model atmospheres.

In case (ii)  $z_0 = \text{const}$ : the discharge is initiated for the charge  $Q$  that fulfils the breakdown criterion  $E(z_0, Q) > E_{\text{th}}$  at a fixed point,  $z_0$ , below the cloud top. This results in the minimum amount of charge,  $Q_{\text{min}}$ , required to initiate a discharge at a fixed point. From this initiation point the discharge propagates into a rising breakdown field. However, due to the enhanced field at the streamer tip it can continue to propagate; therefore, from the point of initiation the propagation is independent of the initial ambient field.

In both cases, (i) and (ii), we assume horizontal homogeneity of the ambient gas; therefore, only the streamer scaling into the vertical direction is considered. This assumption is reasonable since on Earth electric currents flow in the atmospheric electric field preferentially upwards, towards the apex of the geomagnetic field line (Rycroft & Harrison (2012)). The propagating discharge has the form of a sprite-like discharge, starting with only a few branches that split into more and more filaments (Figs. 3).

The discharge propagates through the atmospheric gas according to scaling laws (Sect. 3.4). Each discharge starts with a characteristic diameter and as the discharge evolves and branches, it does so into branches of progressively smaller diameters until the minimum diameter is reached. At this point the whole discharge event stops. This approach follows Ebert et al. (2010a) and their description of streamer behaviour.

### 3.2. Breakdown field

The breakdown field,  $E_{\text{th}}$ , is the minimum threshold electric field that must be overcome in a medium for electrical breakdown to occur. For electric fields above this value, the gas ionisation rate exceeds the electron attachment rate and the ionisation front can propagate. The breakdown field changes depending on the composition of the surrounding medium and the product of the gas pressure and the distance between the electrodes. We use the same description for the breakdown field as in Helling et al. (2013),

$$\frac{E_{\text{th}}}{p} = \frac{B}{C + \ln(pd)}, \quad (1)$$

where  $B$ ,  $C$  and  $pd$  are constants and values are summarised in Helling et al. (2013). Eq. 1 defines the breakdown criterion as a function of gas pressure  $p$  and electrode separation  $d$ . For a given gas composition there exists a critical value of  $(pd)_{\text{min}}$  that yields the minimum electric field strength for electrical breakdown  $E_{\text{th,min}}$ . For values of  $pd < (pd)_{\text{min}}$  the breakdown field  $E_{\text{th}}$  decreases with increasing  $pd$ ; and for values of  $pd > (pd)_{\text{min}}$ , the breakdown field  $E_{\text{th}}$

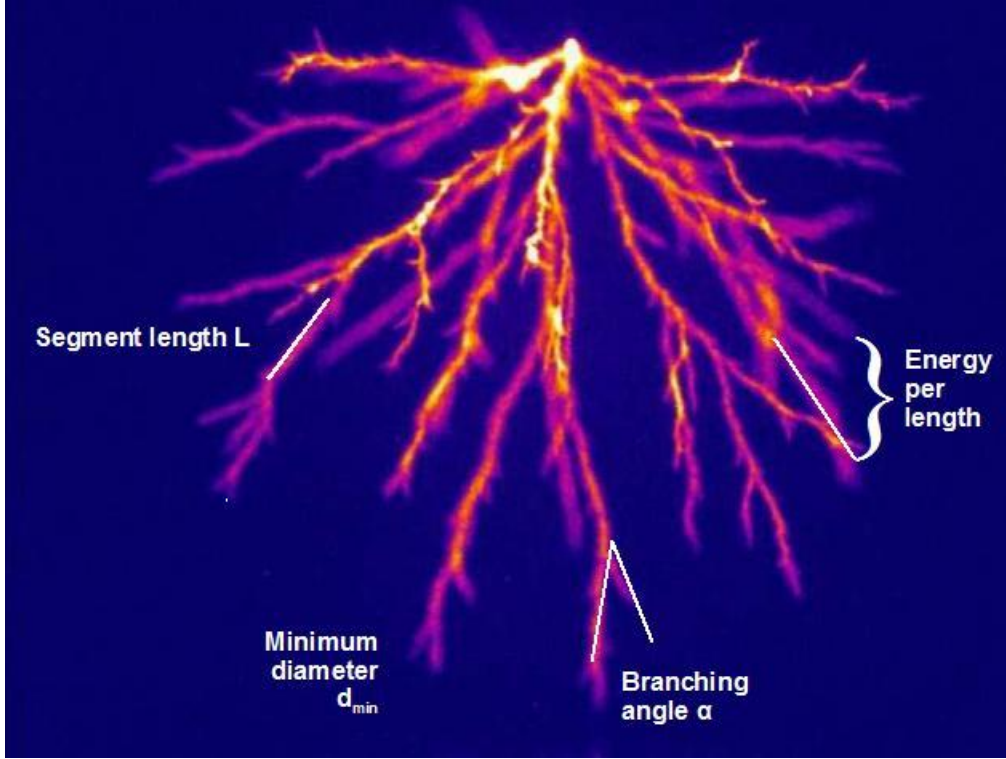


Fig. 3.— This image is adopted from Briels et al. (2008b) [©IOP Publishing. Reproduced with permission. All rights reserved.] to visualise the streamer properties evaluated in laboratory experiments and used in this paper: The segment length,  $L$  (Eq. 6), is the length of a single segment of the streamer. The minimum diameter,  $d_{\min}$  (Eq. 5), is the minimal segment diameter seen on a streamer. The branching angle,  $\alpha$  (Eq. 7), is the angle between two branches from the same parent segment. The energy per length,  $E_{\text{tot}}/l$  (Eq. 8), is the amount of dissipated energy per length of single segment.

increases with increasing  $pd$ . Here, we use the parameters initially determined for Jupiter’s atmosphere (Sect. 4.2). We evaluate the dependence on different chemical composition of the atmosphere in Sect. 5.1.

### 3.3. Model electric field for atmospheric discharges

For simplicity we model the electric field of the cloud with net charge  $Q$  as a simple electric dipole,

$$E(z) = \frac{Q}{4\pi\epsilon_0} \left[ \frac{1}{(z - z_{base})^2} - \frac{1}{(z - z_{top})^2} \right]. \quad (2)$$

A charge distribution within a cloud that has undergone large-scale charge separation can be complex, with opposing layers of charge not always sitting parallel to the horizontal axis but also beside each other due to potentially complex convective cells. Multiple pockets of localised charge distributed across the cloud could also be a likely situation (Rakov & Uman 2003). For simplicity and ease of comparison with similar studies (Raizer et al. 1998; Yair et al. 2009), the dipole electric field in Eq. 2 of two poles (or small pockets of opposite charge) was adopted to emulate a simplified Earth storm cloud cell as suggested by Rakov & Uman (2003). The electric dipole field should provide a fair approximation due to the potentially large distances between the charge centres. Both the local field and the breakdown field are shown in Fig. 4 (for case (ii)):  $Q = Q_{\min}$ , and a discharge starts at the point in the atmosphere where  $E(z) > E_{\text{th}}$ .

The same model is used to study if and where sprites may occur above the cloud at where  $E(z) > E_{\text{th}}$  (Fig. 5). Current sprite theory suggests that these forms of electrostatic discharge occur when charge below is removed suddenly by a lightning stroke, so that a quasistatic field appears above the cloud where a single charge centre remains (e.g. MacGorman & Rust (1998); Briels et al. (2008b)). It is expected that a mirror charge may appear in a conducting ionosphere (see Raizer et al. (1998)); however, no ionospheric considerations have been included here due to lack of knowledge on the nature of ionospheres in brown dwarfs and extrasolar giant gas planets. Sprites occur only milliseconds after powerful lightning strikes within this quasistatic electric field above the cloud.

Although both the local field and the sprite field decay above the cloud, there is a point at which the electrical breakdown condition is satisfied (see Fig. 5). We assume that a sprite launches at this point, triggered by a lightning discharge at lower altitudes.

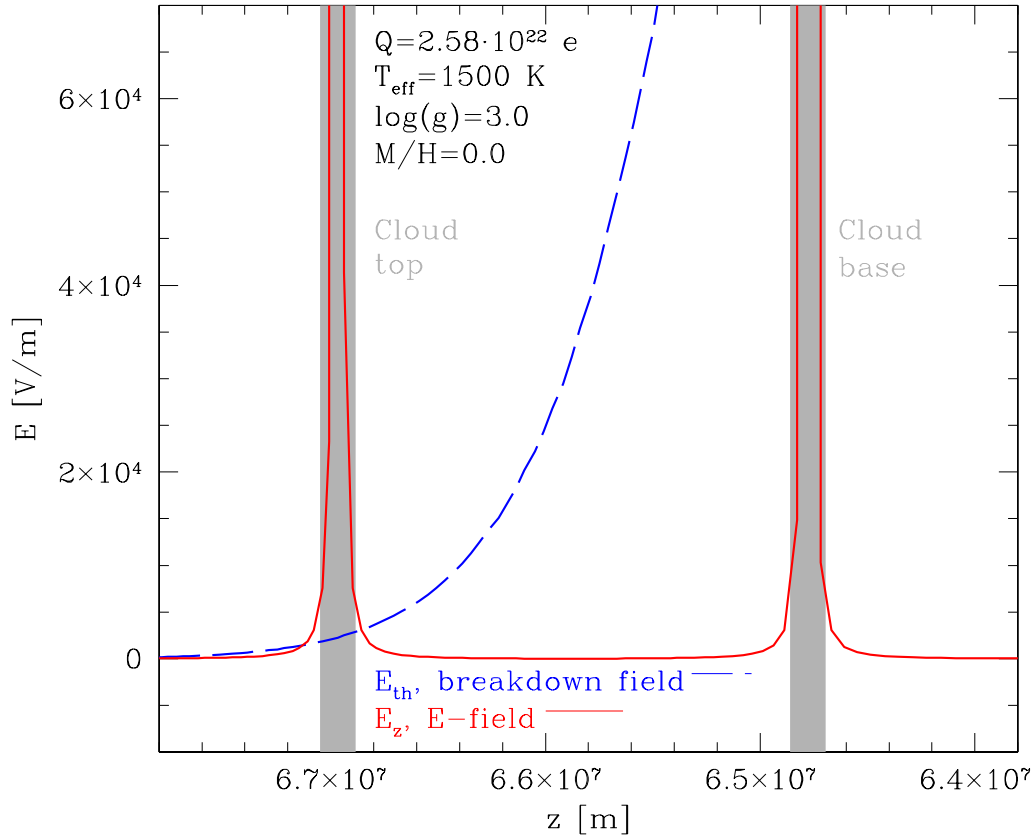


Fig. 4.— The local electric field (red) and the breakdown field (blue) between the charged top and bottom of the cloud layer (depicted in grey) for a DRIFT-PHOENIX giant gas planet atmosphere model with  $T_{\text{eff}} = 1500 \text{ K}$ ,  $\log(g) = 3.0$  and  $[M/H] = 0.0$ . Top and bottom of the cloud are assumed to carry a charge of  $2.58 \times 10^{22} \text{ e}$  of opposite polarity. This is the minimum amount of charge required for a discharge to occur (case (ii)). The discharge occurs at the height  $z$  at which  $E(z) > E_{\text{th}}$ .

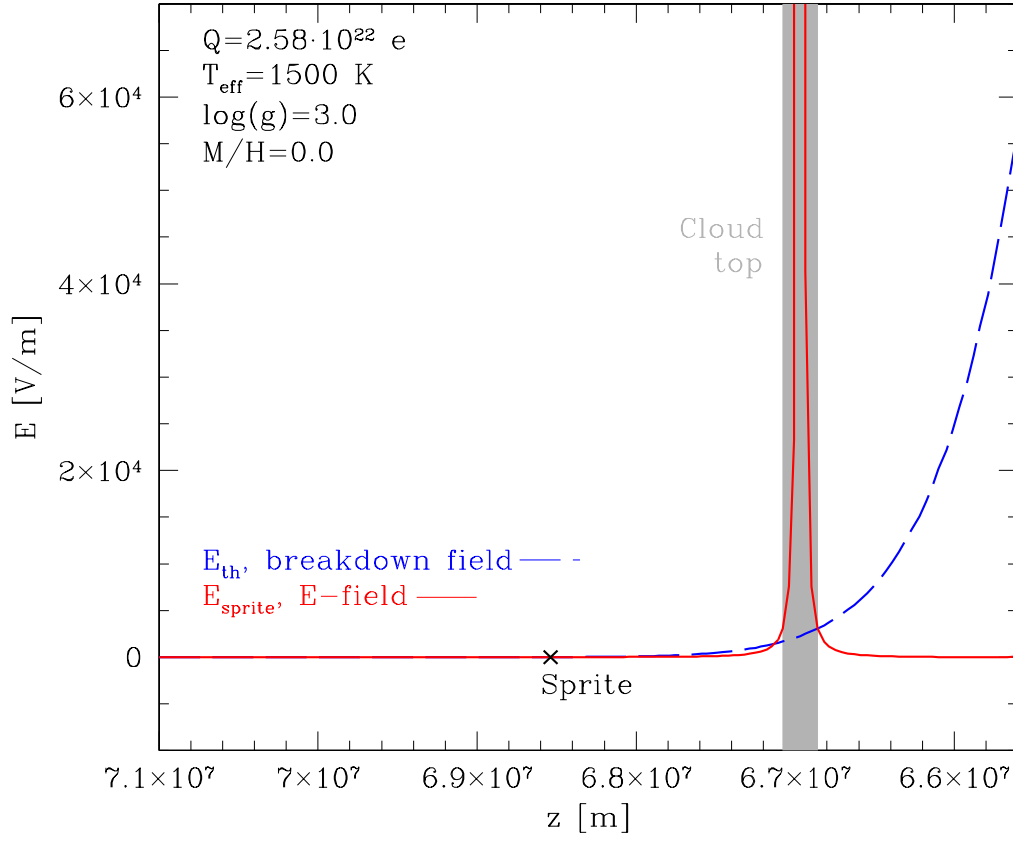


Fig. 5.— The electric field and the breakdown field above the cloud, which is an enlarged portion of the field shown in Fig. 4. At a distance of  $\sim 10^6$  m above the cloud, the electric field exceeds the breakdown field suggesting that a sprite may occur here.

### 3.4. Scaling laws for Streamers and Sprites

Various laboratory experiments in recent years (Briels et al. 2008a,b; Nijdam et al. 2008; Pancheshnyi et al. 2005) studied the properties of the basic discharge instability which occurs in the form of streamers. Streamers are electron avalanches, initiated by fast-moving free ‘seed’ electrons that have been accelerated by a sufficiently strong external electric field. The initial electrons acquire enough energy to knock further electrons from the ambient atom or molecules, which liberate more electrons and the event cascades into an avalanche. This evolves into a self-propagating ionisation front that advances through the medium evolving into a discharge. Laboratory experimental studies of streamers have identified empirical scaling laws that relate characteristic properties of their evolution. This enables us to apply such scaling laws to physically similar systems such as those found in BD and GP atmospheres. Similar investigations have been made in the upper atmosphere of Earth, where the properties of sprites have been quantified (Pasko et al. 1997; Gerken et al. 2000; Cummer et al. 2006; Stenbaek-Nielsen et al. 2007). Sprites, which are massive discharges that occur above thunderstorms milliseconds after powerful lightning strikes, have a similar filamentary structure to streamers. It has therefore been suggested (Briels et al. 2006; Ebert et al. 2010a) that streamers and sprites share similar mechanisms inferring that sprites are streamers scaled to atmospheric pressures.

Empirical scaling laws for the following streamer properties were experimentally determined: the streamer segment lengths ( $L$ ), the minimum diameters ( $d_{\min}$ ), the total energy ( $E_{\text{tot}}$ ) and volume ( $V_{\text{tot}}$ ) of a discharge event (Fig. 3, Briels et al. (2008a,b); Nijdam et al. (2008)). These were found to scale with the gas pressure and applied voltage.

Electron mean free path: The streamer length was observed to scale with the local gas pressure. The physical reason is that a streamer is a flux of electrons travelling through an ambient gas: the mean free path of a single electron before it hits a neutral gas particle is:

$$l_{\text{mfp}} = (\sigma n)^{-1}, \quad (3)$$

and hence,  $l_{\text{mfp}} \propto n^{-1}$  or  $l_{\text{mfp}} \propto p_{\text{gas}}^{-1}$ .  $\sigma$  is the collisional cross sectional area for an electron-neutral interaction and  $n$  is the number density of the gas, which is related to the gas pressure  $p_{\text{gas}}$  by the ideal gas law  $p_{\text{gas}}V = nk_B T_{\text{gas}}$ . This relates to the Paschen curves, which plot the breakdown voltage of a gas as a function of  $pd$ , the product of the gas pressure and separation of the capacitor electrodes (for a summary see Helling et al. 2013). For values of  $pd < (pd)_{\min}$  the breakdown voltage decreases with increasing  $pd$ ; and for values of  $pd > (pd)_{\min}$ , the breakdown voltage increases with increasing  $pd$ .

At high pressures, the mean free path is smaller with respect to the electrode separation resulting in more collisions during the electrons transit between the electrodes. Each collision

randomises the electrons motion and will reduce the electrons energy. This means that the electrons energy may be insufficient to ionise the neutrals it collides with; therefore, requiring a larger voltage to insure sufficient electron energization for electrical breakdown to occur.

At low pressures, the electron mean free path is larger with respect to the electrode separation and the electrons will participate in fewer collisions. In this scenario, the electron may retain its energy but will have fewer collisions requiring a greater breakdown voltage to insure that the collisions that occur are ionising.

The lowest breakdown voltage is found at the value of  $pd$  where these two competing effects balance. While the breakdown voltage depends on the gas pressure, it also depends on the type of gas as each species has a different ionisation energy.

Minimum diameter: The minimum diameter is the minimal width of a streamer segment, below which it does not propagate (Fig. 3). Minimal diameter streamers do not branch into further segments, and are observed at the very final tips of streamers. The assumption that streamers have a minimal diameter is explained in Briels et al. (2008b): the streamer tip consists of a space charge layer, which causes an enhancement of the local electric field. The size of the space charge layer is defined by the inverse of the maximum of the Townsend ionisation coefficient, which is derived from the molecular properties of the gas and changes with pressure. The diameter needs to be larger than this space charge layer to propagate farther, hence there is a minimum possible streamer diameter for a given gas and gas pressure. Most empirically derived relations are of the following form,

$$pd_{min} = A [mm \text{ bar}], \quad (4)$$

The value for the constant  $A$  varies between authors. This relation was tested in detail by Briels et al. (2008b), where they found results of  $A_{air} = 0.20 \pm 0.02$  to  $0.30 \pm 0.02$  in air and  $A_{N_2} = 0.12 \pm 0.03$  in an  $N_2$  gas. Dubrovin et al. (2010) expanded on this by looking at the properties of planetary gas mixtures. For a Jovian mixture they found  $A_J = 0.26 \pm 0.03$ , for a Venusian mixture  $A_V = 0.09 \pm 0.03$  and a value of  $A_{air} = 0.12 \pm 0.03$  in air, similar to Briels et al. (2008b).

Briels et al. (2008b) studied images of sprites in the upper terrestrial atmosphere and evaluated a height-dependent minimum diameter. From this, the dependence of the local gas temperature obeys the relation

$$\frac{pd_{min}}{T} = A \left[ \frac{mm \text{ bar}}{293K} \right]. \quad (5)$$

The temperature dependence in Eq. 5 is predicated on the product  $nd$ , and can be written as  $nd = pd/(k_B T)$  assuming an ideal gas. We note that the ideal gas law can only be

applied to the ambient gas into which the streamer travels, not to the gas that is affected by the streamer. At standard temperature and pressure, Eq. 5 applies to streamers and is consistent with the experimental values in Briels et al. (2008b), supporting the assumption that sprites and streamers are similar in nature.

All experimental works cited below have been performed under normal pressure on the Earth surface ( $\sim 0.1 \dots 1\text{bar}$ ) and for gases of a nitrogen/oxygen mixture or pure nitrogen. Helling et al. (2013) demonstrated that different gas composition do not significantly influence the electric field breakdown in the astrophysical systems studied here. This leads us to assume that the scaling laws applied will not significantly be affected by the different gas-phase composition in our extrasolar atmospheres.

Segment Length: The length  $L$  is the value of the diameter-dependent segment length in air as suggested in Briels et al. (2008b). It describes the distance a single segment travels after a branching event and before the segment itself branches.

$$\frac{L}{d} = 11 \pm 4, \quad (6)$$

with  $d$  being the segment diameter. The values for the segment length,  $L$ , change slightly depending on the gas mixture, and a value of  $9 \pm 3$  was found for streamers in an  $\text{N}_2$  gas. This relation is pressure independent. The error estimates given above result from experimental error estimates given by the referenced authors.

Branching angle: The branching angle,  $\alpha$ , is the angle between new segment branches when a single segment breaks into two new segments. It was investigated by Nijdam et al. (2008) using 3D images of laboratory streamers and the approximately Gaussian distribution with a mean angle was found to be,

$$\alpha = 43.0 \pm 12.3^\circ. \quad (7)$$

The error estimate results from experimental estimates given in Nijdam et al. (2008). We note that streamer channels can also reconnect due to different polarities of the channels (Ebert et al. (2010b)) which we can not take into account in the model presented here. McHarg et al. (2010) observe sprite events above mesoscale thunderstorms and show that propagating streamer heads are both smaller in width and dimmer than splitting streamer heads. The reason for streamer head splitting is the development of a Laplacian instability caused by an increasing electric field in the streamer head (for more details see McHarg et al. (2010)).

Energy: The total energy,  $E_{\text{tot}}$ , of a whole discharge event is calculated by looking at each of the individual segments and their lengths. The value for the total dissipated energy per

length is taken to be (Krider et al. (1968); Cooray (1997); Rakov & Uman (2003)):

$$\frac{E_{\text{tot}}}{l} = 10^5 \text{ J m}^{-1}, \quad (8)$$

with  $l$  a unit length in [m]. The exact number in Eq. 8 depends on the details of the lightning process, e.g. if the first return stroke channel is considered (Cooray 1997). The energy will be dissipated into the heating of the discharge channel and the ambient gas around the channel (e.g. Borovsky 1995). Paxton et al. (1986) suggest that 70% of the total energy input into a channel is optical radiation from the channel. MacLachlan et al. (2013) demonstrate that the energy transfer calculation in a discharge channel needs to take into account a whole variety of collisional processes as for example elastic and inelastic scattering, metastable excitation, ionisation, metastable ionisation, electron-ion recombination. Hence, the precise value in Eq. 8 may differ between authors.

Briels et al. (2008b) observe that the streamer intensity increases with further branching and increasing segment diameter. In comparison, the total energy dissipated per event is estimated to be  $10^7 - 10^9 \text{ J}$  on Earth and  $\approx 10^{12} \text{ J}$  on Jupiter and Saturn.

*Initial diameter:* The behaviour of streamers scaling with voltage was described in Briels et al. (2008a,b), where it was observed that higher voltages led to more intense, longer streamers with thicker branches. The work also showed that the segment diameter increased with increasing voltage, i.e.  $d \propto V$ . However, no empirical relation was derived. Following this result, we assume a voltage dependence to estimate the initial diameter for streamer propagation in our calculations

$$d_{\text{init}} = n_V V_{\text{init}}, \quad (9)$$

where  $n_V = 10^{-8}$  is a constant and is an estimate of the diameter-voltage relation taken from a linear fit to Fig. 5 in Briels et al. (2008b). This expression is of practical interest to us since  $d_{\text{init}}$  determines the final total length of the discharge.

### 3.5. Model for large-scale discharge structures

We adopt the idea that a large-scale lightning strike or a large-scale sprite discharge is composed of multiple streamer events that evolve into such large-scale discharge phenomena. This may not always to be the case and most of the gas-discharges in an atmosphere may in fact not even develop into a streamer as discussed in Helling et al. (2013). However, in this paper we are interested in the scale sizes that large-scale gas-discharge events can occur for in substellar atmospheres assuming that they occur.

The empirical scaling laws for streamers (Sect. 3.4) will be evaluated for the given set of model atmospheres in Sect. 4. After the electric field at a fixed point below the charged cloud top is calculated (Eq. 2), the initial diameter of the streamer,  $d_{\text{init}}$  (Eq. 9), is evaluated. From this initial diameter the streamer branches after each segment length,  $L$  (Eq. 6), into two new segments with a separation angle,  $\alpha$  (Eq. 7). This approach follows Briels et al. (2008a), where bright streamers were described as starting with thick diameters that continued to branch into thinner streamers with smaller diameters until the minimum diameter was reached, at which point propagation stops. The diameters of each new segment follow an area conservation law,

$$d_{\text{new}} = \sqrt{1/2} \frac{d_{\text{old}}}{d_{\text{min,old}}} d_{\text{min,new}}. \quad (10)$$

which depends on the local pressure by Eq. 5. This ensures that lengths are smaller when moving into higher pressures and increase if moving into lower pressures.

To find the minimum diameter of each segment given in Eq. 5, the parameter  $A$  is taken from Dubrovín et al. (2010) for a Jovian atmosphere at room temperature, which we assume to be most similar (hydrogen-based, initially oxygen-rich) to an extrasolar atmosphere,

$$\frac{pd_{\text{min}}}{T} = 0.26 \pm 0.03 \left[ \frac{\text{mm bar}}{293\text{K}} \right]. \quad (11)$$

The total length of the discharge,  $L_{\text{discharge}}$  (distance between the initiation point and termination point of the discharge), and the width of the discharge,  $2W_{\text{discharge}}$ , were evaluated using the segment length given in Eq. 6 and the branching angle in Eq. 7. We assume that the two new branches always split at equal angles of  $\alpha/2$  relative to the vertical axis; therefore,

$$L_{\text{discharge}} = L_0 + \sum_{i=1}^j L_i \cos(\alpha/2) \quad (12)$$

$$W_{\text{discharge}} = \sum_{i=1}^j L_i \sin(\alpha/2), \quad (13)$$

where  $j$  is the total number of steps the discharge takes (where a step is defined as the point at which a new layer of segments has branched out of the old), so that the total number of segments in any step is given by  $2^j$  and  $L_0$  is the length of the initial, solitary segment.

The total number of segments,  $N_{\text{segment}}$ , was also evaluated as it is related to the total energy. It was calculated by adding the number of branches over each step,

$$N_{\text{segment}} = \sum_{i=0}^j 2^i. \quad (14)$$

The volume of the discharge can be derived in two ways: a) The cone volume  $V_{\text{cone}}$  (Eq. 15), which is simply the volume filled by the cone of a height and width taken from the results of Eqs. 12 & 13 formed by the discharge branches, and b)  $V_{\text{total}}$  (Eq. 16), which is the sum over the total number of individual segments of the discharge, each of which has been treated as a simple cylinder,

$$V_{\text{tot}} = \frac{1}{3} \pi W_{\text{discharge}}^2 L_{\text{discharge}} \quad [m^3] \quad (15)$$

$$V_{\text{segments}} = \sum_{i=0}^j 2^i \left( \frac{\pi d_i^2}{4} L_i \right) \quad [m^3]. \quad (16)$$

The total dissipated energy,  $E_{\text{tot}}$ , is calculated in a similar fashion: it is the sum over the total number of segments, where the length of each segment is multiplied by the energy per length given in Eq. 8,

$$E_{\text{tot}} = \sum_{i=0}^j 2^i (10^5 L_i) \quad [J]. \quad (17)$$

## 4. Results

In this section, we discuss the results of our model for large-scale discharges (see Sect. 3.5) for brown dwarf (BD) and gas giant (GP) model atmospheres, and for their subsolar ( $[M/H] = 0.0$ ) and sub-solar ( $[M/H] = -3.0$ ) metallicity counterparts. We investigate how these scales change with global model parameters like the effective temperature ( $T_{\text{eff}} = 1500 - 2000\text{K}$ ). The range of effective temperatures considered comprises those extrasolar, low-mass objects where dust clouds form inside the atmosphere and determine the observable spectrum. As outlined in Sect. 3.1, the results are derived by two different methods:

Case (i) The first method compares the results for each model atmosphere for a constant total number of charges ( $Q_1 = 6.24 \times 10^{21}$  e and  $Q_2 = 3.12 \times 10^{22}$  e) Using a prescribed number of charges, the maximum distance from the cloud top of a possible discharge initiation within the cloud was found by searching for the point in the cloud at which  $E_{z, Q_{\text{const.}}} > E_{\text{th}}$ . This

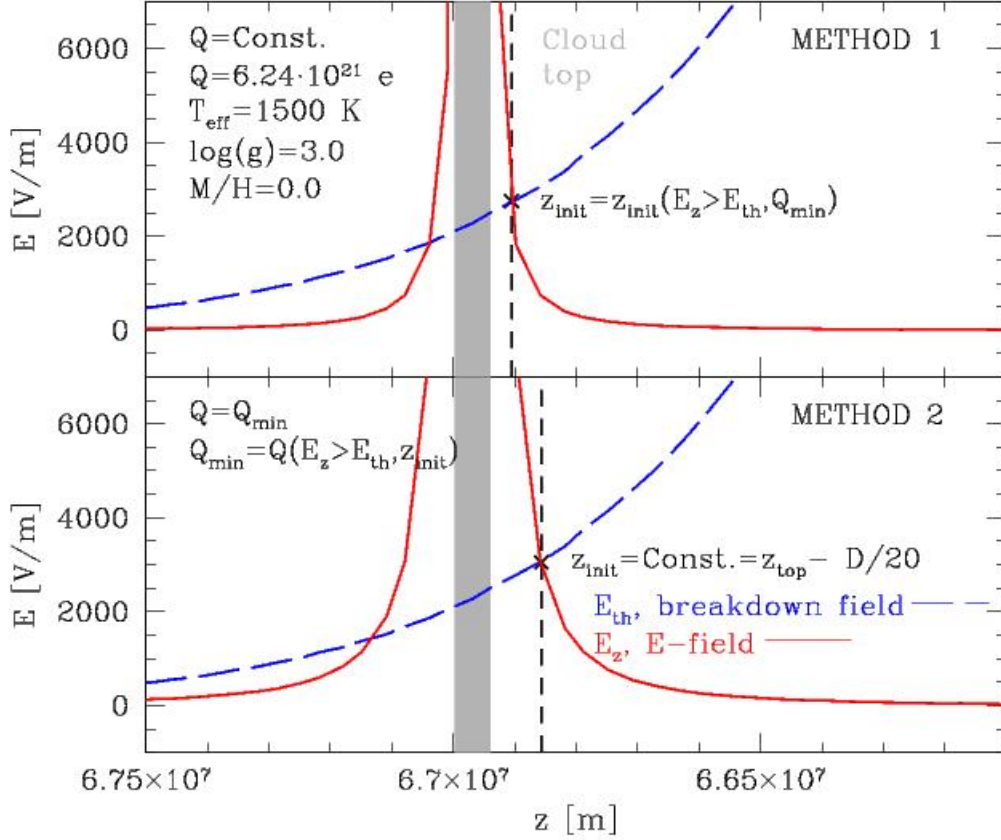


Fig. 6.— Electric fields for the emerging large-scale discharges within gas giant and brown dwarf atmospheres (break-down field – dashed blue line; local electric field – solid red line). **Top** (case (i)): The total number of charges is prescribed (shown for  $Q_1 = 6.24 \times 10^{21} \text{ e}$ ). **Bottom** (case (ii)): Atmospheric altitude of discharge onset is prescribed which allows to determine a minimum total charge needed for the break-down to occur ( $Q_{\text{min}} = 2.58 \times 10^{22} \text{ e}$  for the model shown). The DRIFT-PHOENIX model atmosphere parameters are  $T_{\text{eff}} = 1500 \text{ K}$ ,  $\log(g) = 3.0$ , and  $[M/H] = 0.0$ .

point is  $z_{\text{init}}$ . The top panel in Fig. 6 shows  $z_{\text{init}}$  for the DRIFT-PHOENIX model atmosphere of a giant gas planet ( $T_{\text{eff}} = 1500$  K,  $\log(g) = 3.0$ ) of initial solar metallicity ( $[M/H]=0.0$ ).

Case (ii) The second method compares the results for the minimum amount of charge,  $Q_{\text{min}}$ , required for a discharge to occur at a point  $z_{\text{init}}$  below the cloud top for each individual model atmosphere. To evaluate comparable minimum charges for each atmosphere, a set point of discharge initiation below the cloud top was put at a distance 1/20th the height of the cloud:  $z_{\text{init}} = z_{\text{top}} - (\Delta H/20)$ , where  $\Delta H$  is the height of the cloud. Discharges would initiate at the bottom of this layer, and the minimum amount of charge,  $Q_{\text{min}}$ , required to overcome the breakdown field at that point was found such that  $E(z_{\text{init}}, Q_{\text{min}}) = E_{\text{th}}$ . From there, the discharge was allowed to propagate assuming the value of initial minimum charge was present in the cloud region. The bottom panel in Fig. 6 shows  $E(z_{\text{init}}, Q_{\text{min}}) = E_{\text{th}}$  for the DRIFT-PHOENIX model atmosphere of a giant gas planet ( $T_{\text{eff}} = 1500$  K,  $\log(g) = 3.0$ ) of initial solar metallicity ( $[M/H]=0.0$ ).

The two-fold evaluation process is necessary because we do not know *a priori* how many charges are available in the atmosphere. For the same reason, Raizer et al. (1998); Pasko et al. (2000) and Yair et al. (2009) assume the presence of a certain number of charges at the height in their atmospheres under investigation. In contrast, calculations for the Earth’s atmosphere are somewhat guided by *in situ* measurements.

#### 4.1. Minimum Charges for electrical breakdown

We first evaluate the minimum charge required in a cloud layer for a discharge to initiate just below the cloud top (case (ii), bottom panel 6). The results for the different model atmospheres are shown in Fig. 7: the amount of charge required to initiate a discharge decreased from the cool atmospheres to the hotter atmospheres. This arises as a consequence that the cloud decks form at lower pressures (hence lower gas temperatures) as the effective temperature increases. In analogy with a classical breakdown in a capacitor discharge, our atmosphere system is operating in the regime  $pd > (pd)_{\text{min}}$ , where  $d$  is the electrode’s separation. This means for a fixed  $d$  and a decreasing gas pressure that the required breakdown voltage, and hence the corresponding  $Q_{\text{min}}$ , decreases. Therefore, if  $T_{\text{eff}}$  increases we expect  $Q_{\text{min}}$  to decrease.

The breakdown field depends only on gas pressure  $p$  and chemical composition of the gas parametrised by some constants characterising the discharge. In this study, we are assuming that  $\text{H}_2$  is the most abundant gas species in the atmosphere and so the breakdown conditions are defined for a  $\text{H}_2$ -dominated gas. However, the chemical composition of low-metallicity

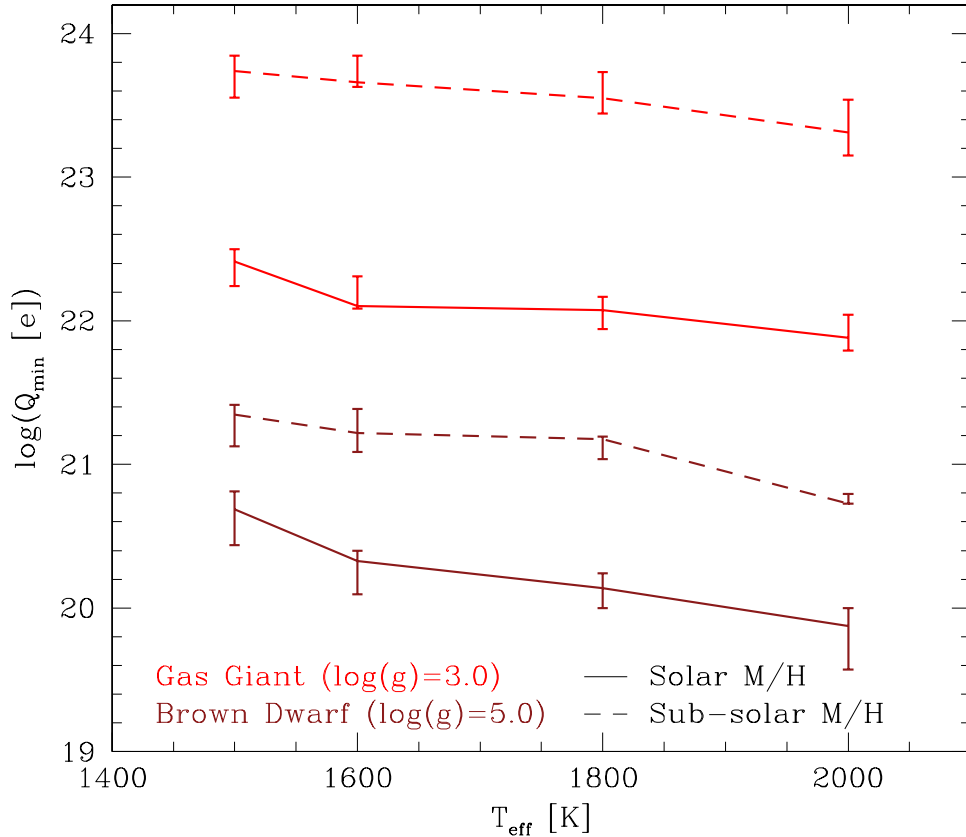


Fig. 7.— The minimum charge,  $Q_{\min}$ , required to initiate a discharge in model atmospheres of different effective temperatures,  $T_{\text{eff}}$  for BDs (brown) and GGs (red) and for different metallicities (solar = solid line, subsolar = dashed line). Independent data points are connected to visualise potential trends in the results. Due to pressure differences in the cloud layers, the brown dwarfs require less amounts of charge than the gas giants, and in both cases the lower-metallicity atmosphere models require greater amounts of charge than the solar-metallicity atmospheres. The error bars indicate the uncertainty with which the cloud height is determined based on the DRIFT-PHOENIX atmosphere models (see also Sect 5.2).

atmospheres will differ to the solar case. Although  $\text{H}_2$  remains the most abundant gas-phase species, other molecules will be less abundant, which has an impact on the thermodynamic structure of the atmosphere due to radiative transfer effects: low-metallicity atmospheres are generally more compact for a given temperature compared to their solar counterparts which causes the clouds to form at higher pressures (but lower temperature) in low-metallicity atmospheres. Therefore, the metal abundances have an indirect influence on  $Q_{\min}$ : we find that  $Q_{\min}$  is larger in low-metallicity atmospheres since the clouds form at higher pressure and require a greater breakdown voltage.

Figure 7 suggests that GP atmospheres require larger amounts of charge to initiate an electric breakdown of the gas. However, referring back to Fig. 1, we see that the BD clouds form at higher pressures, which should lead to the BDs having large values of  $Q_{\min}$ . This discrepancy is caused by the vertical extension of BD clouds, which have extensions of only  $10^4$  m in comparison to the  $10^7$  m clouds in the GP atmospheres. The small extension causes the field to be larger throughout the cloud in comparison to the GP case. This leads to BD models needing lower amounts of charge to initiate a field breakdown due to the comparatively larger local electric fields.

## 4.2. Large-scale discharge properties

This section evaluates the initiation height of the discharge in the atmosphere; the total length of a discharge event; the total number of segments that compose the discharge event; the atmospheric volume affected by the discharge; and the total energy per discharge dissipated into the atmosphere. All quantities are evaluated for various sets of DRIFT-PHOENIX model atmospheres defined by: the effective temperature, the gravitational acceleration and the metallicity ( $T_{\text{eff}} = 1500, 1600, 1800, 2000$  K,  $\log(g) = 3.0, 5.0$ ,  $[M/H] = 0.0, -3.0$ ).

### 4.2.1. Initiation height

We evaluate the discharge initiation height,  $z_{\text{init}}$ , for a given number of charges ( $Q_1 = 6.24 \times 10^{21}$  e and  $Q_2 = 3.12 \times 10^{22}$  e) as the height below the cloud top where the local electric field exceeds the breakdown threshold field, i.e. where  $E(z) > E_{\text{th}}$  is satisfied. Results for all the atmospheric types are plotted in Fig. 8, where the two separate point types represent the two charge amounts. Increasing the prescribed charge increases the local electric field strength, allowing the local breakdown field to be overcome in regions of higher pressure. As a result, since the gas pressure increases with distance below the cloud top, the distance

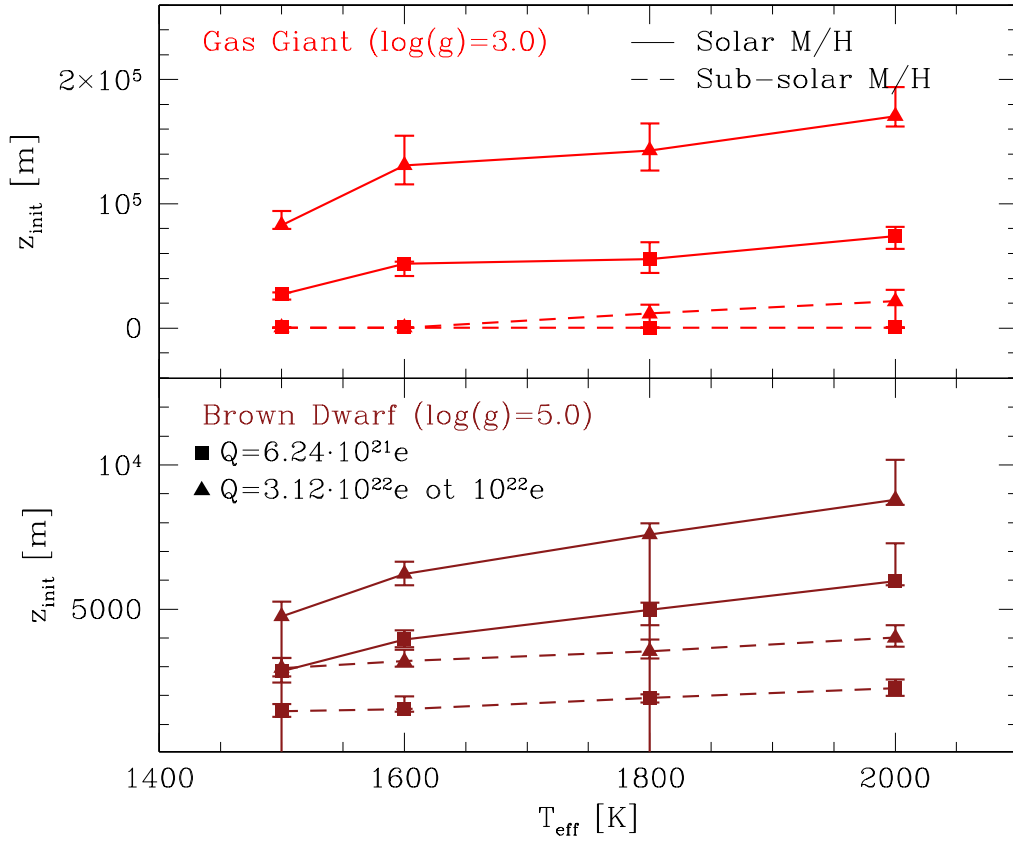


Fig. 8.— Distances between the cloud top and the discharge initiation height,  $z_{\text{init}}$ , the point at which the local electric field grew larger than the breakdown threshold field ( $E(z) > E_{\text{th}}$ ) for different atmosphere models (top - GPs ( $\log(g)=3.0$ ), bottom - BDs ( $\log(g)=5.0$ )). Results are shown for two different value of number of charges (squares:  $Q_1 = 6.24 \times 10^{21} \text{e}$ ; triangles:  $Q_2 = 3.12 \times 10^{22} \text{e}$ ) and for a solar metallicity (solid lines) and a sub-solar metallicity (dashed line) case. The error bars indicate the uncertainty with which the cloud height is determined based on the DRIFT-PHOENIX atmosphere models (see also Sect 5.2.)

from the cloud top for a discharge initiation,  $z_{\text{init}}$ , will increase. Furthermore, an increase in effective temperature causes the discharge initiation height to move further into the cloud, i.e. into regions of higher gas pressure. Cloud regions in hotter atmospheres form at lower pressures (i.e. higher up in the atmosphere) with increasing  $T_{\text{eff}}$  (compare Fig. 1), and the local electric field in these clouds (for a constant number of charges) is greater than the breakdown field for a greater distance into the cloud.

The behaviour of the low metallicity GP stands out in these plots as the initiation distance from the charges is nearly coinciding with the charge carrying cloud top, where the field is very large. As shown in Fig. 7, minimal charges of the order of  $10^{23}$  e were required to initiate a discharge in these low-metallicity atmospheres due to the cloud tops forming at comparatively higher pressures, hence deep inside the atmosphere. This means that the only region in which a discharge could realistically initiate is directly on the charge carrying surface, where the field is near-infinite. In this scenario, the dipole electric field model is insufficient to model the system since the initiation point is in such close proximity to the charged surface that the spatial distribution of charge and the resulting field effects would need to be considered. This may suggest that discharges would not occur in sub-solar metallicity cloud models for the given number of charges ( $Q_1 = 6.24 \times 10^{21}$  e,  $Q_2 = 3.12 \times 10^{22}$  e) assumed in Fig. 8.

#### 4.2.2. Total discharge lengths

The total discharge lengths for the two different cases of a prescribed number of charges (case (i)) and for a calculated minimum charge,  $Q_{\text{min}}$ , to start a electrical breakdown (case (ii)) are shown in Figs. 9. Both cases demonstrate that discharges can be expected to be much more extended in a brown dwarf atmosphere than in a giant gas planet atmosphere ( $10\times$  the GP values) if both are considered to result from the same number of charges (left of Fig. 9).

Figure 9 shows that a large-scale discharge can propagate over  $0.5 - 4$  km which is strongly dependent on the metallicity and surface gravity. Our results suggest that high-pressure atmospheres, due to high surface gravity or low metallicity, produce exceptionally large discharges: low-metallicity atmospheres and brown dwarfs seem to have the largest total discharge length. The high pressure results in a small mean free path and more collisions occurring during the electron transit between the cloud ‘electrodes’. Each collision randomises the electron motion and will reduce the electron energy. Therefore, for an atmosphere with higher pressure, the magnitude of the electric field required to initiate electrical breakdown is greater. Following the empirical scaling relations, this implies that the initial

breakdown potential is greater and hence the size of the initial diameter of the subsequent streamer:  $d_{\text{init}} = n_V V_{\text{init}}$ . As a consequence, as the streamer propagates through the atmosphere and begins to branch, the length of the resulting streamer segments will be greater since  $L \propto d$ . Therefore, we expect discharges to have a greater spatial scale in high pressure atmospheres such as brown dwarfs. Furthermore, for a high pressure atmosphere we would expect the minimum diameter ( $d_{\text{min}} \propto T/p$ ) to be small, enabling the streamer to propagate for a greater distance before the minimum diameter is reached.

Therefore, a high-pressure gas will allow for the streamer process to progress over a longer distance through an ambient gas while it will die out quickly in a low-pressure environment. Therefore, *lighting discharges can be expected to be larger, and therefore easier to detect, in brown dwarfs and low-metallicity planetary atmospheres.* Although a larger volume would be affected, less radiation may be emitted due to a lower number of collisions due to lower densities, unless a saturated process dominates the emission process. The dependence on the effective temperature is not very strong if  $Q = \text{const}$  as in Figs. 9.

All of the total discharge propagation lengths decrease with increasing effective temperature. The total lengths in the  $T_{\text{eff}}=2000$  K atmospheres were in some cases 50% the total discharge length in a  $T_{\text{eff}}=1500$  K model atmosphere. The primary reason is a large geometrical extension of the cloud in the hotter atmospheres leads to a lower electric field value for the same amount charge, which results in a smaller discharge length. A higher number of total charges led to larger discharge lengths in all model atmospheres considered. Comparing the BD model discharge lengths between the  $Q = \text{const.}$  and  $Q = Q_{\text{min}}$  models (Figs. 9) produces a similar conclusion supporting this result: the minimum number of charges required to initiate discharges in BD atmospheres were of the order of  $10^{20} - 10^{21}$  e, much smaller than the charges applied in Fig. 9 (case (i)).

#### 4.2.3. Total number of segments

We evaluate the the total number of segments (or branches),  $N_{\text{segments}}$  (Eq. 14), that compose the whole discharge event in the atmosphere. Figure 10 shows  $N_{\text{segments}}$  for a prescribed constant number of total charges (top plot) and shows  $N_{\text{segments}}$  for the minimum number of charges needed for field break-down (bottom plot). Both figures suggest an almost exponential decrease of the number of branches across all atmospheres, and that they are much more numerous in the low-metallicity atmospheres.

The number of segments grows exponentially with the total length of the discharge. If a discharge reaches greater lengths, it may branch more often. The behaviour of  $N_{\text{segments}}$

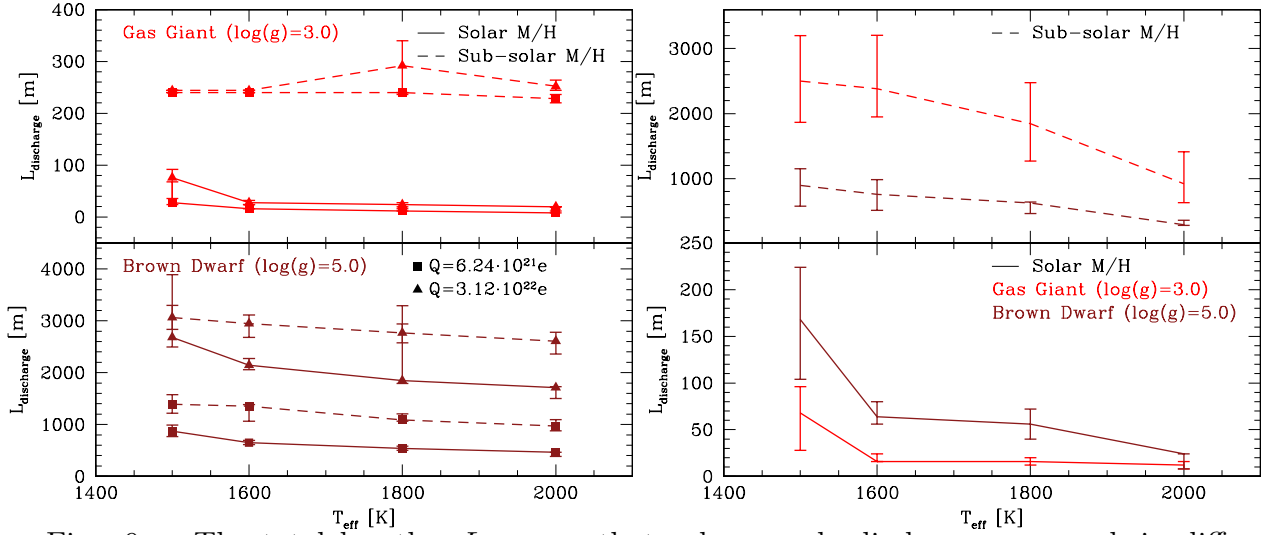


Fig. 9.— The total lengths,  $L_{\text{discharge}}$ , that a large-scale discharge can reach in different atmospheres (top - GPs ( $\log(g)=3.0$ ), bottom - BDs ( $\log(g)=5.0$ )) with solar metallicity (solid lines) and a sub-solar metallicity (dashed line). **Left:** Results for two different value of a constant number of charges (squares:  $Q_1 = 6.24 \times 10^{21} \text{ e}$ ; triangles:  $Q_2 = 3.12 \times 10^{22} \text{ e}$ ). **Right:** Results for the minimum number of charges needed for a field break-down. The error bars indicate the uncertainty with which the cloud height is determined based on the DRIFT-PHOENIX atmosphere models (see also Sect 5.2).

is similar to that of the total discharge length: higher pressure atmospheres (due to higher gravitational acceleration or lower metallicity) require a higher breakdown voltage, resulting in a larger  $d_{\text{init}}$ , larger segment lengths  $L$  and a lower  $d_{\text{min}}$ . Therefore a large-scale discharge with a greater spatial extent is more likely to have a greater number of segments.

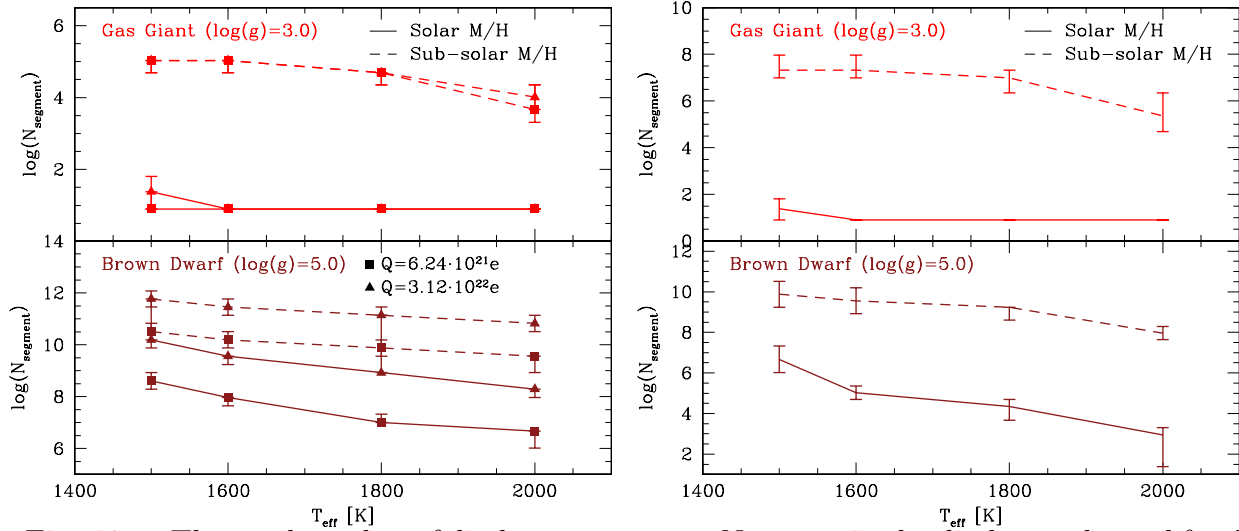


Fig. 10.— The total number of discharge segments,  $N_{\text{segments}}$ , in the discharge channel for different model atmospheres (top panels - GPs ( $\log(g)=3.0$ ), bottom panels - BDs ( $\log(g)=5.0$ )). All results are shown for a solar metallicity (solid lines) and a sub-solar metallicity (dashed line) case. **Left:** results for two different value of a constant number of charges (squares:  $Q_1 = 6.24 \times 10^{21} \text{ e}$ ; triangles:  $Q_2 = 3.12 \times 10^{22} \text{ e}$ ), **Right:** results for minimum charges needed for field breakdown. The error bars indicate the uncertainty with which the cloud height is determined based on the DRIFT-PHOENIX atmosphere models (see also Sect 5.2).

#### 4.2.4. Total energy dissipated

We now estimate the total energy dissipated by a large-scale discharge event in a sub-stellar atmosphere. We utilise the total dissipation energy per length,  $E_{\text{tot}}$  in units of  $[\text{J/m}]$  (Eq. 8), and combine it with our estimate for the number of segments,  $N_{\text{segment}}$  (Eq. 14), and the length of each of these segments,  $L$  (Eq. 6), which leads to Eq. 17. We note, however, that the factor of  $10^5$  in Eq. 8 may vary for different atmospheric chemistries. Our investigation of the electric break-down conditions in (Helling et al. 2013) show, however, that the gas-phase composition does only introduce small differences.

We evaluate the total dissipated energies (Eq. 17) depending on the model atmosphere parameters  $T_{\text{eff}}$ ,  $\log(g)$ , and on metallicity. This is done for both cases: (i) for a constant

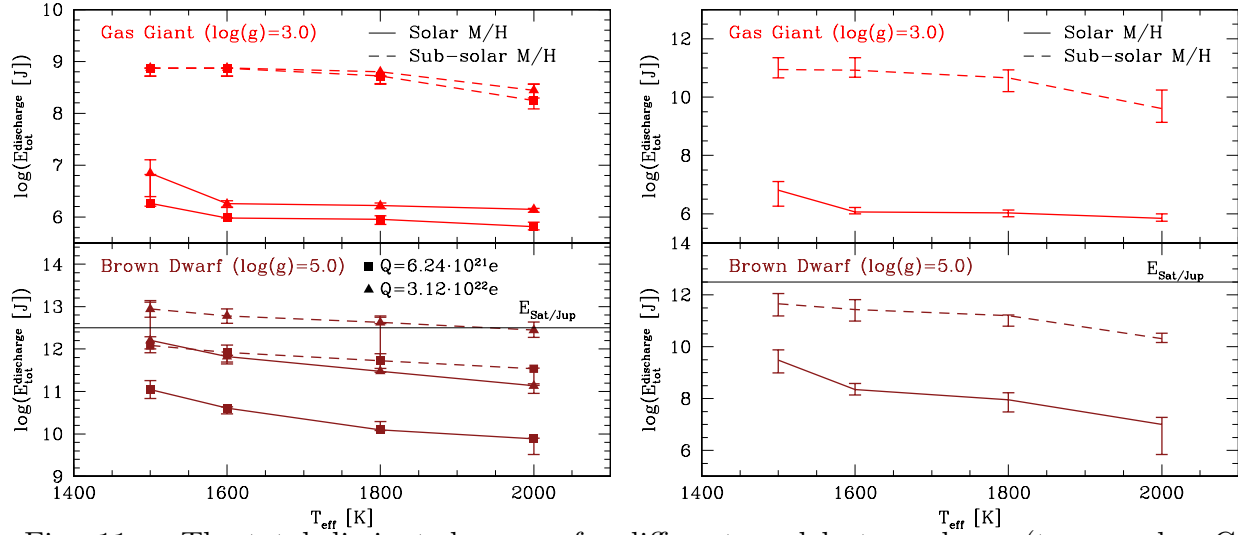


Fig. 11.— The total dissipated energy for different model atmospheres (top panels - GPs ( $\log(g)=3.0$ ), bottom panels - BDs ( $\log(g)=5.0$ )). All results are shown for a solar metallicity (solid lines) and a sub-solar metallicity (dashed line) case. **Left:** results for two different value of a constant number of charges (squares:  $Q_1 = 6.24 \times 10^{21} \text{ e}$ ; triangles:  $Q_2 = 3.12 \times 10^{22} \text{ e}$ ), **Right:** results for minimum charges needed for field breakdown. The error bars indicate the uncertainty with which the cloud height is determined based on the DRIFT-PHOENIX atmosphere models (see also Sect 5.2).

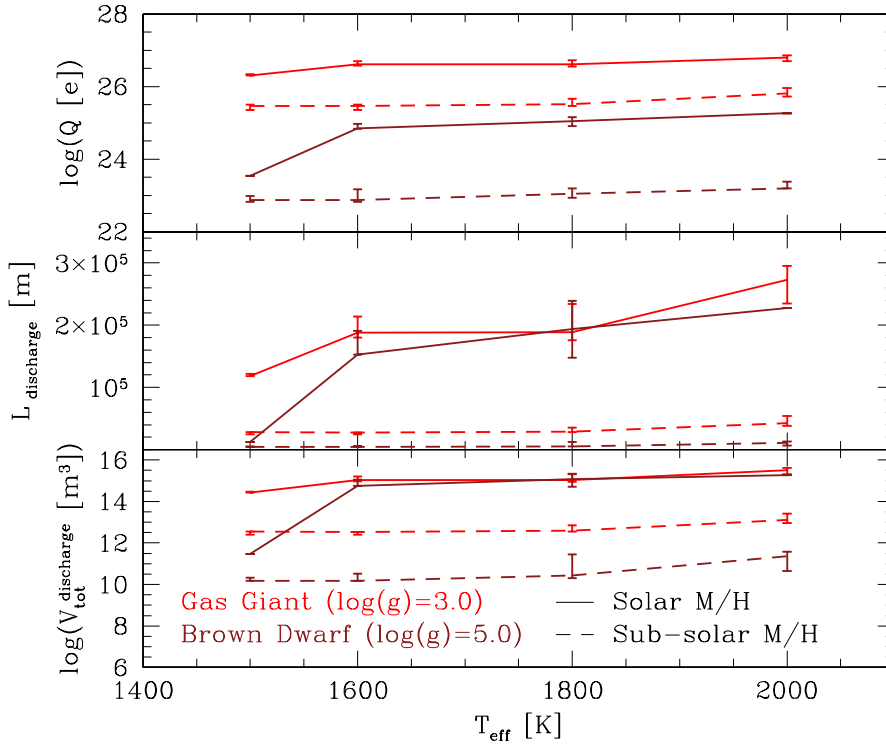


Fig. 12.— Characteristic discharge values for a given total dissipation energy,  $E_{\text{tot}} = 10^{13}$  J. **Top:** The minimum charge,  $Q_{\text{min}}$  [e], needed to achieve a field-breakdown with a total dissipation energy  $E_{\text{tot}} = 10^{13}$  J ( $E_{\text{tot,Jupiter}} = 10^{12} \dots 10^{13}$  J,  $E_{\text{tot,Saturn}} \approx 10^{12}$  J); **Middle:** Total propagation length,  $L_{\text{discharge}}$  [m], of the large-scale discharge dissipating  $E_{\text{tot}} = 10^{13}$  J.; **Bottom:** Total atmospheric volume affected by the propagating discharge that dissipates a Jupiter/Saturn equivalent of  $E_{\text{tot}} = 10^{13}$  J. All values are shown for different model atmospheres. The error bars indicate the uncertainty with which the cloud height is determined based on the DRIFT-PHOENIX atmosphere models (see also Sect 5.2).

number of charges; and (ii) the minimum charges for each atmosphere. The results in Fig. 11 demonstrate that the total dissipated energy is of the order of  $10^6 - 10^9$  J for solar metallicity atmospheres. These values are comparable to typical solar system values which are  $E_{\text{tot,Earth}} = 10^8 - 10^9$  J,  $E_{\text{tot,Venus}} = 10^9 - 10^{10}$  J,  $E_{\text{tot,Jupiter}} = 10^{12} - 10^{13}$  J, and  $E_{\text{tot,Saturn}} \approx 10^{12}$  J. Our estimates suggest that more energy is released in a brown dwarf atmosphere than in a giant gas planet because of the large dissipation length. The total dissipation energy in our example GP atmospheres is generally more comparable to the lightning dissipation energy on Earth. However, the total dissipated energy reaches its highest values of  $10^{10} - 10^{13}$  J for the low-metallicity objects, which had both higher values of  $Q_{\text{min}}$  and longer total discharge lengths than their solar metallicity counterparts, leading therefore to higher energies.

For a better comparison with known solar system values of energies of  $10^{12}$ - $10^{13}$  J in Saturn’s and Jupiter’s atmospheric discharges, the discharge propagation model was ran with increasing applied charge (similar to the constant charge case) until a Jupiter/Saturn equivalent dissipation energy of  $E_{\text{tot}} = 10^{13}$  J was reached. The results plotted in Fig.12 show that larger lengths are required in the hotter atmospheres to reach the same amount of dissipated energy. This confirms our previous result for a constant charge, that smaller discharge lengths should occur in hotter atmospheres compared to cooler atmospheres (Sect. 4.2.2).

Our results also demonstrate in Fig. 12 that a geometrically larger downward-propagating discharge would be required in a GP atmosphere than in a brown dwarf in order to achieve the same dissipation energy in both objects. Similarly, the discharge length is smaller in the low-metallicity atmospheres compared to the solar-metallicity atmospheres.

This later test of finding the discharge properties for a given total dissipation energy leads us to conclude that our results are consistent within the framework of our discharge scaling model. Our model is based on scaling laws derived from laboratory and numerical experiments on streamers. However, we can not exclude the possibility that other processes, not quantified by the experimental studies, can affect the the amount of energy dissipated or the length scale of the discharge process.

#### 4.2.5. Total discharge volume

The volumes of atmosphere affected by a discharge propagating through the atmospheric gas was treated as a cone filled by the discharge branches as defined in Eqs. 15 and 16. The results for constant charges are shown in Fig. 13 (left), and those at  $Q_{\text{min}}$  in Fig. 13 (right). For discharges of the size of  $10^2$  m (GP) and  $10^3$  m (BD, see Fig. 9), we observe total cone

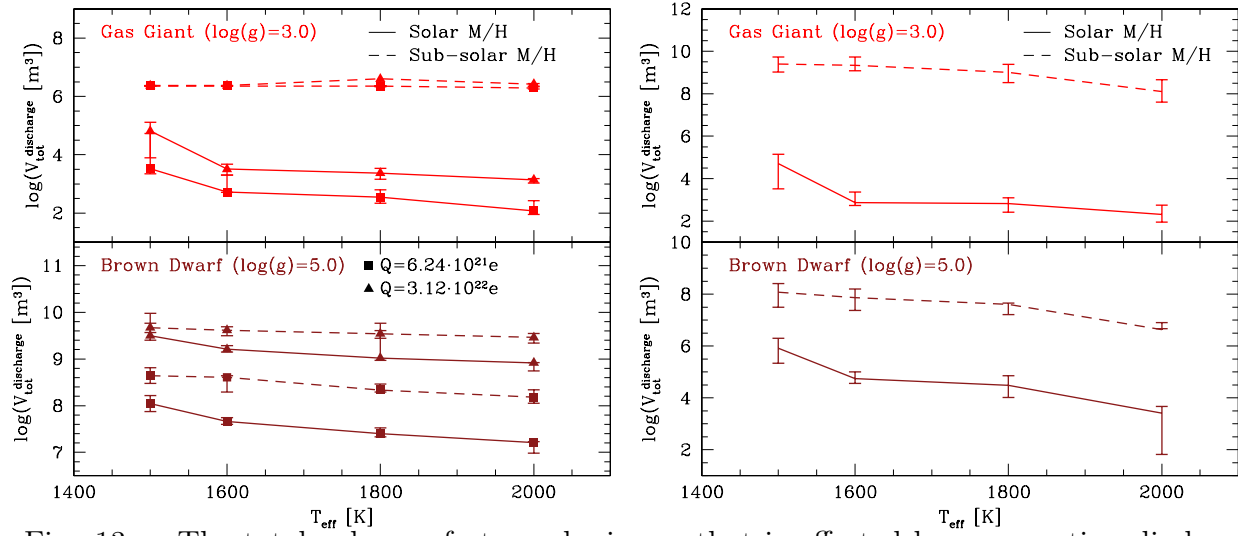


Fig. 13.— The total volume of atmospheric gas that is affected by propagating discharges through the atmospheres studied. **Left:** for two constant charges ( $Q_1 = 6.24 \times 10^{21} \text{ e}$ ,  $Q_2 = 3.12 \times 10^{22} \text{ e}$ ), **Right:** the minimum charges. The error bars indicate the uncertainty with which the cloud height is determined based on the DRIFT-PHOENIX atmosphere models (see also Sect 5.2).

volumes of the orders of  $10^4 - 10^6 \text{ m}^3$  and  $10^8 - 10^{10} \text{ m}^3$  respectively. This is the estimated volume of the atmospheric gas where a population of ions, metastables and electrons has been injected in the streamer wake. Combined with the local electric field and associated change in local temperature, this will allow chemical reactions not normally permitted in the ambient atmosphere.

However, the volume of the atmospheric gas that is exposed to the discharge may be underestimated in our simplistic scaling model. For example, a fractal ansatz for discharge propagation as suggested in (Pasko et al. 2000) might yield larger volume values.

### 4.3. Sprites

Streamer discharges are suggested to determine the early stages of lightning discharges and of sprites (Phelps (1974); Raizer (1991); MacGorman & Rust (1998); Briels et al. (2008a)). Sprites, which are massive discharges that occur above thunderstorms milliseconds after powerful lightning strikes (and are therefore also referred to as *above-cloud discharges*), have a similar filamentary structure to streamers. It has therefore been suggested (e.g. Briels et al. (2006) and Ebert et al. (2010a)) that streamers and sprites share similar underlying

physical mechanisms. Massive *National Lightning Detection Networks* provide evidence that sprites and lightning discharges are linked: About 80% of the observed sprites on Earth coincide with lightning ground strokes (Boccippio et al. 1995). This is confirmed by numerical modelling in combination with high-speed measurements of sprite optical emissions in Liu et al. (2009) and Gamerota et al. (2011), as well as by dedicated observation campaigns for single events (Füllekrug et al. (2013))

An electromagnetic pulse that results from a very large cloud discharge in the Earth’s atmosphere can transfer (positive) charges downwards. The consequence is a large electrostatic field above the thundercloud that exceeds the (classical) threshold electric field for breakdown and creates an upward directed sprite discharge (e.g. Rycroft & Harrison (2012)). The classical breakdown field (Sect.3.2) does generally not incorporate the idea of a runaway breakdown as described in e.g. Roussel-Dupré et al. (2008), and therefore overestimates the critical field strength needed for electrical breakdown to start. However, the classical approach can still provide guidance for first-order-investigations as performed in this paper in order to gain insight into how sprite extensions may change in different, extrasolar environments.

The comparison of the local electric field resulting from a large-scale charge distribution with the critical (classical) break-down field (Fig. 5) shows that the local electric field can exceed the breakdown field below and above the charge-carrying cloud layer. This indicates that the discharge process can start downwards into the cloud and along a positive density gradient *and* upwards above the cloud travelling into a negative density gradient. The downwards travelling discharges could be considered equivalent to intra-cloud lightning on Earth, and the upward directed discharge resulting in an upward travelling ionisation front could be considered equivalent to a sprite.

The electric field for a possible sprite, as shown in Fig. 5, was evaluated in the regions above the cloud deck in the different cloud-forming model atmospheres considered here. Figure 14 shows at which height above a cloud top a sprite would initiate for brown dwarfs and giant gas planets of different  $T_{\text{eff}}$ . The condition for the appearance of sprites is the same as that for other discharges considered here, namely that the electric field above the cloud charge distribution must be larger than the breakdown field. Figure 14 therefore plots at which height above the cloud  $E_{\text{init, sprite}} > E_{\text{th}}$ . This method was used by Yair et al. (2009) to investigate the possibility of Sprites in other solar system planets than Earth.

Figure 14 (left) only contains results for the models describing atmospheres of giant gas planets because the electric field strength exceeds  $E_{\text{th}}$  for all locations above the cloud in brown dwarf atmospheres. Hence, sprites would potentially appear at any height above the cloud layer in a brown dwarf. A similar behaviour occurs in giant gas planet atmospheres

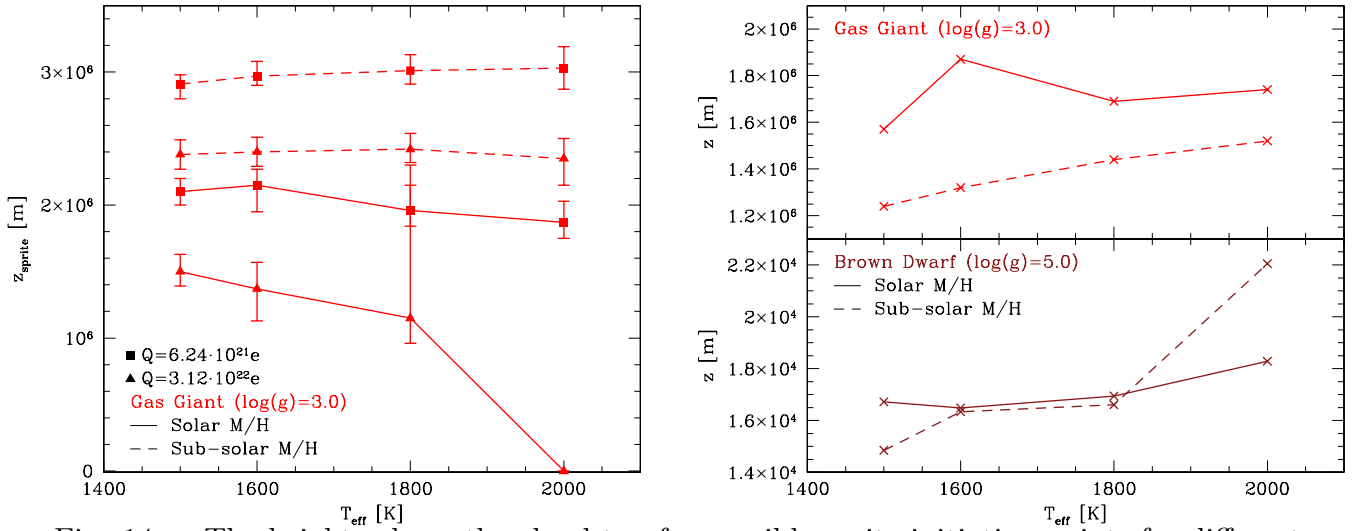


Fig. 14.— The heights above the cloud top for possible sprite initiation points for different model atmospheres (red - GPs ( $\log(g)=3.0$ ), brown - BDs ( $\log(g)=5.0$ )). All results are shown for a solar metallicity (solid lines) and a sub-solar metallicity (dashed line) case. **Left:** results for two different value of a constant number of charges (squares:  $Q_1 = 6.24 \times 10^{21} \text{ e}$ ; triangles:  $Q_2 = 3.12 \times 10^{22} \text{ e}$ ), **Right:** results for minimum charges needed for field breakdown. The error bars indicate the uncertainty with which the cloud height is determined based on the DRIFT-PHOENIX atmosphere models (see also Sect 5.2).

(Fig. 14, left) where for an increasing number of charges, hence an increasing electric field strength, sprites appear closer and closer to the cloud top. The distance from the cloud top dropping to zero in the solar metallicity  $T_{\text{eff}} = 2000$  K atmosphere signifies the same result as that for the BDs: that a sprite could occur at any point above the cloud.

A less straight forward behaviour occurs if the minimum charges for field break-down is considered (Fig. 14, right): the distance from the cloud top increases slightly as the effective temperature rises.

The total gas volume affected by one streamer should intuitively be larger than a traditional lightning-affected volume because a Sprite can travel much further. However, it is not obvious how the column density would differ between a lightning and a Sprite discharge because of the outward negative density gradient in an atmosphere. In the framework of our streamer propagation model, we can not evaluate the atmospheric gas volume affected by a sprite as the diameter of the discharge channels increase as they propagate into lower pressure regions. Our method diverges for sprites (Eq. 4) because we utilise the existence of a minimum streamer diameter as termination criterion for streamer propagation. This is appropriate for streamer propagation along a positive pressure gradient into an atmosphere. If the streamer propagates along a negative pressure gradient, its diameter increases and its propagation would be terminated by the increasing mean free path of the avalanche electrons which at some point will not have enough energy to travel further. However, this process is not incorporated by our simple streamer propagation model.

## 5. Uncertainty assessment of large-scale discharge properties

### 5.1. The influence of the gas composition

All of the above results were calculated for DRIFT-PHOENIX model atmospheres using the parametrisation for the breakdown field  $E_{\text{th}}$ , for the chemical composition of a Jupiter atmosphere (Helling et al. 2013). This is inconsistent in comparison to the initial solar or subsolar element abundances used in the atmosphere models. We therefore assess in how far different chemical compositions of the atmospheric ionising gas may change our results.

First, we calculate the minimum charges,  $Q_{\text{min}}$ , needed to achieve a local electric field larger than the threshold breakdown field for the different atmospheres, *assuming* an atmospheric gas that has a composition comparable to Earth, Mars, Venus, Saturn (parameters used from (Helling et al. 2013)). The results are plotted in Fig. 15 for giant gas planet atmospheres ( $\log(g) = 3.0$ ) of solar composition ( $[M/H] = 0.0$ ) and for different effective temperatures. The charge needed to initiate electrical breakdown is largest in an Earth-like

$\text{N}_2$ -dominated atmospheric gas; and smallest in a atmosphere of a Jupiter-like  $\text{H}_2$ -dominated composition. The results may reflect the higher ionisation energy of  $\text{N}_2$  (15.5808 eV) compared to  $\text{H}_2$  (15.4259eV). However, the difference between these two values is not very large, which leads us to refer to the effect of so-called Penning-mixtures (or neon lamp effect). The effect here is that the gas contains a species which is easier to ionise than the most abundant species; hence, it efficiently seeds the field breakdown at lower voltages. In general, the numbers are not significantly different between the different atmospheric gases.

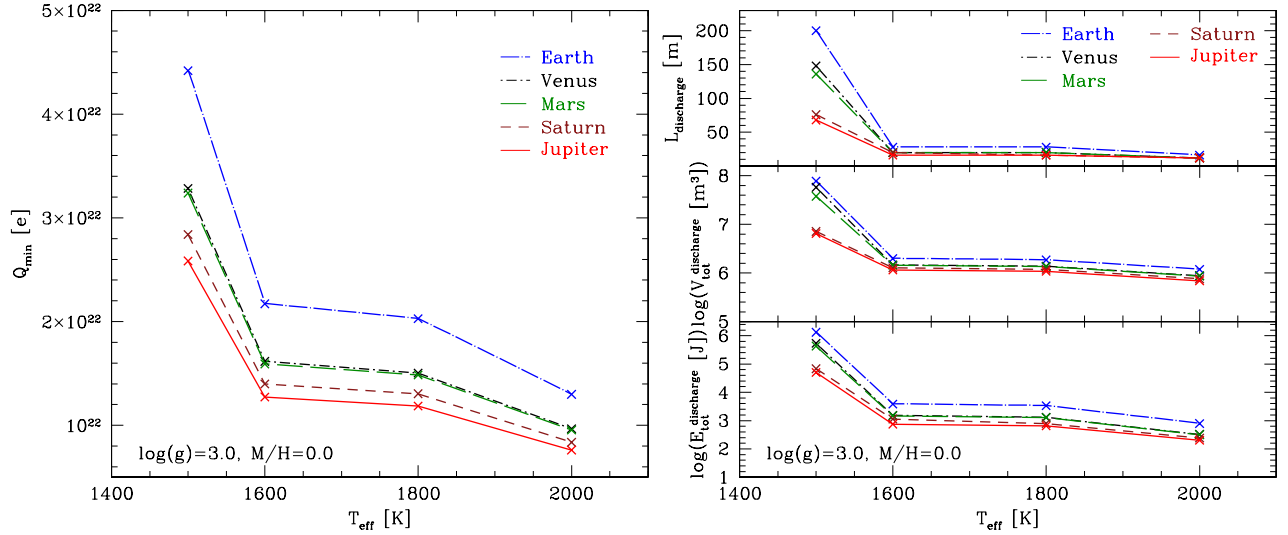


Fig. 15.— Dependence of large-scale discharge properties on chemical composition that influences the break-down values of atmospheric gas for different  $T_{\text{eff}}$ . **Left:** The minimum charge,  $Q_{\text{min}}$ , required to overcome the breakdown field at every point in the atmosphere for ionising gases of different chemical composition. **Right:** The total discharge length  $L_{\text{discharge}}$  (top), the total volume  $V_{\text{tot}}^{\text{discharge}}$  (centre), and the total energy  $E_{\text{tot}}^{\text{discharge}}$  (bottom) are plotted for different discharge chemistries with each minimum charge as shown on the left of this figure. Venus and Mars lie very close. We evaluate giant gas planet atmospheres ( $\log(g) = 3.0$ ) of different  $T_{\text{eff}}$  and solar metallicity ( $[M/H] = 0.0$ ).

Using these minimum charges in Fig. 15, we show what effect different atmospheric chemistries might have on the total propagation length of the discharge (total discharge length),  $L_{\text{discharge}}$ ; the total atmospheric volume affected by the discharge ionisation,  $V_{\text{tot}}^{\text{discharge}}$ ; and the total energy dissipated into the surrounding gas,  $E_{\text{tot}}^{\text{discharge}}$  (left of Fig. 15).

The total propagation length of the whole discharge event does not change appreciably with the chemical composition of the gas for the higher-temperature models. Given the differences in  $L_{\text{discharge}}$  and the total atmospheric volume affected by the discharge ionisation,

$V_{\text{tot}}^{\text{discharge}}$ , it is only logical that the total dissipation energy is higher in an Earth-like atmosphere compared to Jupiter. The effect of the different atmospheric chemical compositions appear to have the largest impact on the discharge properties of the low-temperature models.

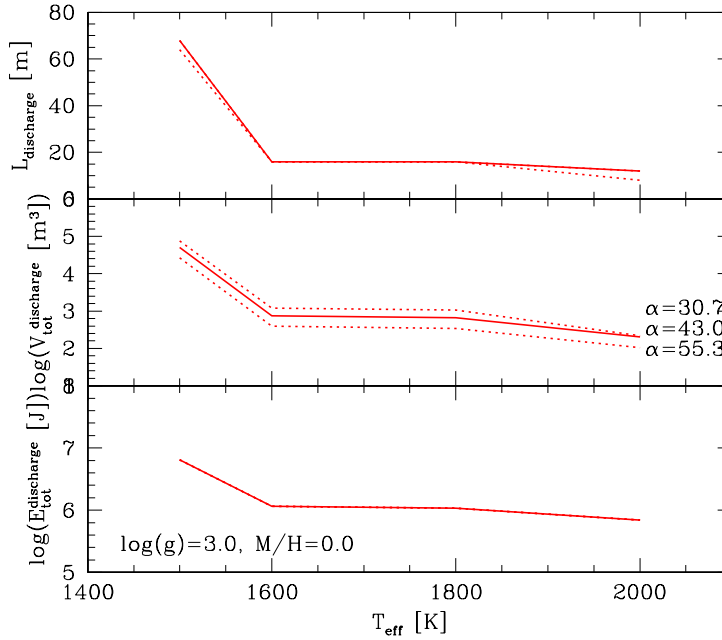


Fig. 16.— Dependence of large-scale discharge properties on different branching angles. **Top:** discharge lengths, **Middle:** volume of the discharge cone, **Bottom:** total dissipated energies. The dotted lines represent the upper and lower limits of the branching angle (Nijdam et al. 2008). The results are for atmospheres with  $\log(g) = 3.0$ ,  $[M/H] = 0.0$ .

## 5.2. The influence of experimental uncertainties

All our estimates in the previous section are based on laboratory experiments and evaluation of numerical results. We assess the uncertainties introduced by the somewhat large uncertainties in the branching angle,  $\alpha$ , and by the determination of the cloud boundaries from the DRIFT-PHOENIX model atmospheres.

*Branching angle  $\alpha$ :* The branching angle was given by Nijdam et al. (2008) with an error estimate of  $\alpha = 43.0 \pm 12.3^\circ$  (Sect. 3.4). Figure 16 demonstrates how this uncertainty

affects the values for total lengths, energies and volumes using the minimum charge model,  $Q_{\min}$ . Each upper and lower limit for each  $\alpha$  is plotted. The total dissipation energy is not affected; the total discharge length show small variations; and the total volume affected by the discharge shows an uncertainty of approximately half an order of magnitude.

*Cloud boundary:* Cloud boundaries in the DRIFT-PHOENIX atmosphere models were derived by looking at the nucleation maximum that defines the cloud top, and a lower and upper cloud boundary was defined for each. In the gas giants, the corresponding error spans  $\approx 10^5$  m; and in the brown dwarfs these errors were of the order of  $\approx 10^3$  m due to the smaller cloud sizes. The program was run for the same conditions as the original points, for each upper and lower limit to find the difference. These limits are represented by the error bars on the plots. (Figs. 7- 14 (left)). Although these errors can be large, the principle findings of our study do not change. Moreover, the resulting errors on the total dissipation energy (Fig. 11) and the total volume affected by one large-scale discharge event (Fig. 12) are small.

## 6. The effect of electrical discharge events on the local gas chemistry

Atmospheric electric discharge events, and associated physicochemical interactions, are highly non-equilibrium processes. The accelerated electrons, those of the streamer, ionise the ambient medium creating a significant population of ions, radicals, metastable species and additional electrons. Driven by the prevalent local electric field permeating the medium, chemical reactions are allowed that would normally be forbidden in a solely thermally-driven system. Such non-equilibrium plasma chemistry is complex and formidable to model. To simplify matters, we focused our attention to timescales where the generated plasma species was extinguished, which left us with a heated volume of thermalised gas as result of the discharge event. As the gas cooled, we looked at the subsequent quasi-static equilibrium states and the resulting chemistry as a function of time.

We present a tentative, initial discussion of the effect that energy dissipated by a discharge event (in a discharge channel) has on the atmosphere, the atmospheric chemistry and the local gas-phase composition. We assume that the gas-phase chemistry remains in steady state, hence, all gas-phase kinetics proceed on time-scales shorter than  $\tau_{\text{chem}} = 10^{-4}\text{s}$ . However, this may be incorrect for some of the species considered as outlined in e.g. Lorenz (2008). Similar attempts have been made to investigate the atmospheric chemistry of the Earth and other solar-system planets. For example, Kovács & Turányi (2010) investigated the evolution of Titan’s chemistry as a result of lightning strikes. Kovács & Turányi (2010) considered a lightning channel gas cylinder of diameter 0.025 m and of initial maximum

temperature 30000 K. The plasma in the lightning column extinguished quite rapidly, but the gas temperature decreased on a longer time scale. This intense heating of the lightning channel is observed as optical emission in Earth and on Jupiter (e.g. Zarka et al. 2004). Kovács & Turányi (2010) numerically solved the heat conductivity equation in order to calculate the time-dependent temperature cooling profile of the lightning channel (their Fig. 1). Titan has a different chemical composition than the extrasolar objects considered in this paper; however, the principle physical mechanisms of an electrical breakdown are the same, independent of the local difference in chemistry. Foreseeable differences in time-scales can result from the chemistry dependent cooling efficiency, particularly in rich gas mixtures (e.g. Fig. 12 in Voitke et al. 1996). Such time-scale effects are not too important for our study as our main interest is the changing temperature during the cooling process.

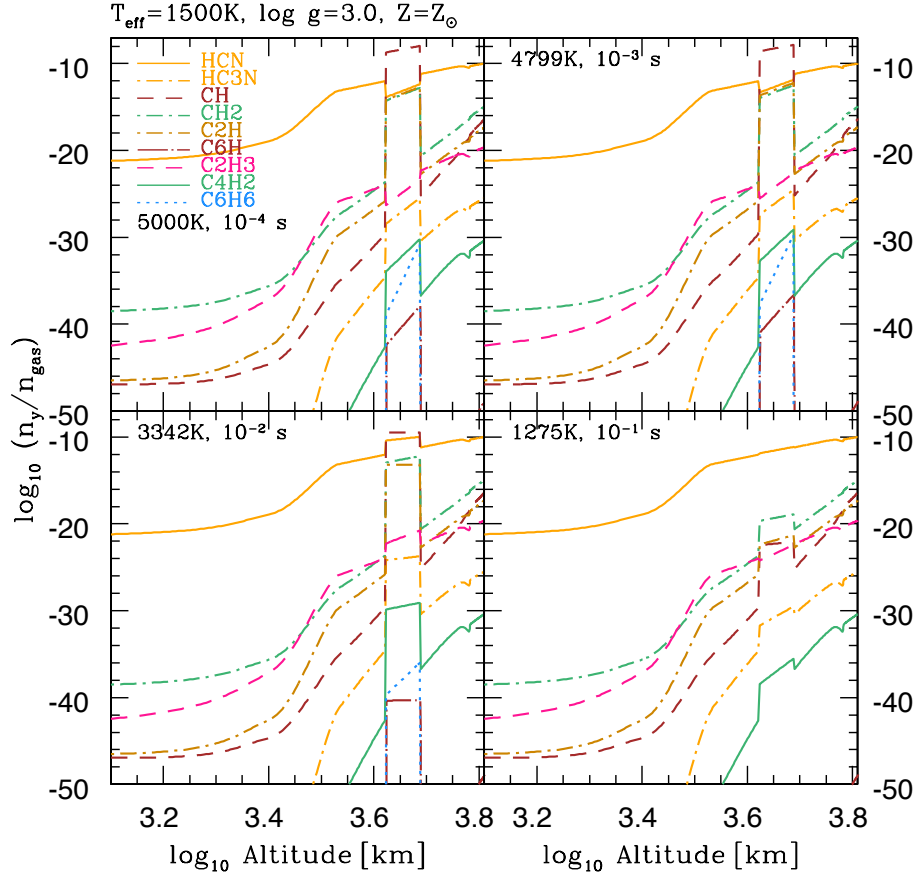


Fig. 17.— Carbon molecules concentrations at different times after a lightning event in the cloud layer of a giant gas planet model atmosphere ( $T_{\text{eff}} = 1500$ ,  $\log(g)=3$ , solar). The figure panels follow the post-lightning temperature profile from Kovács & Turányi (2010).

We started our chemistry calculations from a DRIFT-PHOENIX atmosphere model for

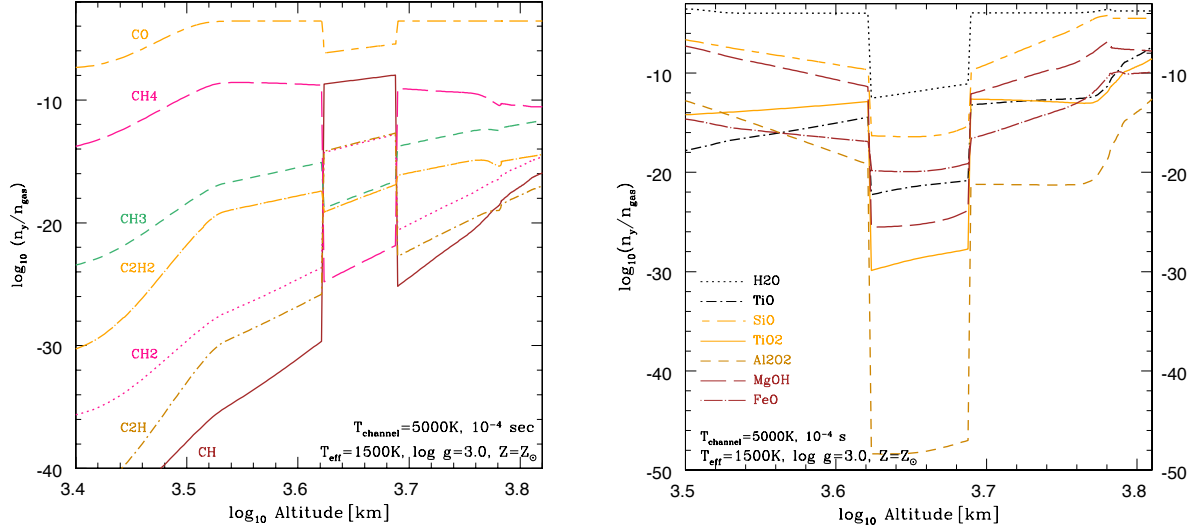


Fig. 18.— **Left:** A blow-up for the small hydrocarbon molecule concentration in a gas heated by lightning discharge to 5000K,  $10^{-4}$  s after the initiation of the ionisation front. Note the increase of CH and C<sub>2</sub>H in expense of CH<sub>4</sub>. **Right:** Same for oxygen-binding molecules which participate in cloud particle condensation. H<sub>2</sub>O is only indirectly affected by cloud formation, namely by the depletion of oxygen.

a giant gas planet ( $T_{\text{eff}} = 1500$  K,  $\log(g)=3$ , solar). We discuss possible changes of the gas-phase composition due to changed thermal conditions of the atmospheric region that was affected by a lightning discharge. The time-dependent temperature decrease after the lightning event is directly adopted from Fig. 1 in Kovács & Turányi (2010).

The lightning channel inside the dust cloud of our example gas-giant atmosphere affected the atmospheric gas at heights bracketed by  $T_{\text{gas}} = 930$ K and  $T_{\text{gas}} = 1088$ K (plotted as  $z$ -values in Figs. 17 and 18), which is equivalent to a atmospheric volume of  $\sim 10^{13}$  m<sup>3</sup>. We applied a chemical equilibrium routine to evaluate the vertical profiles of C-bearing molecules (Figs. 17, 18) and of molecules that are involved in the cloud particle condensation process (Fig.18, right) by mimicking the effect of an electrical breakdown by the enhancement of the local gas temperature. Each panel in Figure 17 represents a different time after the electric discharge occurred, and hence a different channel temperature: 5000K (0.0001 seconds), 4799K (0.001 seconds), 3342K (0.01 seconds) and 1275K (0.1 seconds). The sharp edges correspond to the discontinuity in the temperature profile, which suddenly rises to 5000K, for example. The production of certain carbonaceous species is hindered by these high gas temperatures: the high temperature breaks the stable molecules such as methane and carbon monoxide into radicals, which may recombine to form molecules that are more stable at high temperatures (e.g. CH, C<sub>2</sub>H, HC<sub>3</sub>N). These results generally agree with the lightning model

of Kovács & Turányi (2010) for Titan. We did, however, not reproduce the increase in the concentration of  $\text{C}_2\text{H}_6$ , and did not measure a significant production of HCN, one of the proposed chemical products of lightning (e.g. Lorenz 2008; Hurley et al. 2012). This is an indication that the chemical equilibrium approach is not appropriate for reactions affecting these molecules. Indeed, the after-lightning concentrations of HCN,  $\text{C}_2\text{H}_2$  and  $\text{C}_2\text{H}_3$  only increase for a lower channel temperature of 3342K.

The oxygen-bearing molecules underwent a decrease in their abundances for every channel temperature considered, and also  $\text{H}_2\text{O}$  is dissociated at such high temperatures. The decreased abundances of molecules like TiO, SiO,  $\text{SiO}_2$ , MgOH, and FeO suggests a sudden stop of potential condensation processes, hence, a freeze-in of the dust properties (e.g. grain sizes), unless the high-temperature time span is sufficiently long to evaporate the cloud particles completely.

The analysis presented here is a tentative investigation of the effects of electrical discharges on atmospheric chemistry. It is by no means an exhaustive study. This work is a first step to see which kind of differences in the gas-phase chemistry could be expected due to the extreme temperature changes during a discharge event in extrasolar atmospheres. Inspired by the Miller-Urey experiment, our interest was to see if large carbon-binding macro-molecules could be affected in the frame of our ansatz. This is a first step to identify chemical species as a possible spectral fingerprint for extrasolar lightning.

## 7. On the observation of lightning in extrasolar atmospheres

Lightning and cosmic rays are important sources providing electrons to the terrestrial **atmosphere** and the ionosphere. Lightning will play a comparable role in Brown Dwarfs and exoplanets contributing to the pool of non-thermal electrons that can accelerate along magnetic field lines or that participate in coherent plasma motion, both producing, for example, radio and X-ray emission. Such radio and X-ray radiation was detected in brown dwarfs and is thought to origin from accelerated electrons (Berger et al. 2010; Hall 2002; Burgasser et al. 2011, 2013; Route & Wolszczan 2013; Williams et al. 2013a,b; Cook et al. 2013).

Nearby brown dwarfs that are not hiding inside a host-stars magnetosphere are an easier target than exoplanets to detect radio emission that originates from lightning directly (e.g. WISE1541: 2.8pc, GJ845Ba&b: 3.6pc; Belu et al. 2013). Further, the brown dwarfs known to us are at much closer distances than known extrasolar planets. The nearest brown dwarf is the binary ( $\text{L}8\pm1$  /  $\text{T}1\pm1$ ) Luhman 16 (WISEJ1049) at a distance of  $\sim 2\text{pc}$  which is a factor

of  $5\times$  less than the distance assumed in Zarka et al. (2012). Luhman 16 (and other brown dwarfs) have been suggested to show cloud-related variability (Gillon et al. 2013) in the T-dwarf component, but no radio observations are available yet for this object. The brown dwarf binary 2MASSJ1314 (L5/T7) has been reported to show hyperactive quiescent radio emission (Burgasser et al. 2013). Williams et al. (2013a) present the first quiescent radio emission from a T dwarf (T6.5, 2MASS J1047), which demonstrates that radio emission is detectable from the coolest of the brown dwarfs. This radio emission is thought to arise from gyrosynchrotron emission potentially pointing towards the presence of a weak chromosphere, however, other mechanisms can not be ruled out yet. Non-equilibrium (like cosmic rays, Rimmer & Helling 2013) or dynamic ionisation processes (Alfvén ionisation, Stark et al. 2013) were suggested in addition to lightning discharges to play a significant role in feeding the atmospheric *plasma* in ultra-cool, low-mass objects to interact with its magnetosphere in order to explain the origin of this radiation.

To predict observable signature for lightning itself is not a trivial task as atmospheric electrical discharges produce broad-band observable signatures across the electromagnetic spectrum. Direct emission results from the afore mentioned acceleration of electrons (radio, X-ray and gamma-ray emission) and the excitation of atomic states, such as metastable states (IR, optical emission) during the discharge process. Indirect emission results from the effect on the local chemistry due to the electrified environment or the associated acoustic shock. Additional emission as a consequence of secondary effects, such as the triggering of sprites and energetic electron beams, are also possible and have been detected for terrestrial lightning storms on Earth (Füllekrug et al. 2013).

Research on discharge observables has focused on single events in the Earth atmosphere and atmospheres in the solar system. Table 1<sup>2</sup> summarises these signatures and links them to astronomical instruments according to their wavelength capacity (right column). Which signature might appear in which exoplanet’s or brown dwarf’s atmosphere depends on the atmospheric composition, temperature, element abundance, and maybe velocity fields. The effect of the discharges on the local chemistry manifests in the higher or lower abundance of certain molecules<sup>3</sup> as we show in Sect. 6. A sensible assessment of potential spectral

---

<sup>2</sup> Terrestrial Gamma-ray Flashes (TGFs) are brief (typically  $< 1$  ms) bursts of  $\gamma$ -rays with a mean energy of 2 MeV originating from the Earth’s atmosphere (Lu et al. 2011). Both  $\gamma$ -ray and X-ray emissions are consequences of the production of energetic runaway electrons by lightning (Dwyer et al. 2012). *Sferics* (or *atmospherics*) are radio emissions in the low-frequency range with a power density peak at 10 kHz on Earth. Whistlers are electromagnetic waves propagating along magnetic field lines and emitting in the VLF range. The effect of the discharges on the local chemistry manifests in the higher abundance of certain molecules.

<sup>3</sup> For example, the largest natural source of nitrogen-oxyds in the Earth’s troposphere is lightning (Yair

signatures for planets other than solar-system-twins will require a radiative transfer solution similar to the synthetic spectrum analysis done in model atmosphere simulations.

## 8. Concluding summery

Fossil evidence suggests lightning has influenced the Earth’s atmosphere for at least 250 million years (Harland & Haker 1966). It has also been speculated that lightning could be responsible for synthesising the first prebiotic molecules in a young Earth’s atmosphere (Miller & Urey 1953, 1959; Johnson et al. 2008). Stark et al. (2013) demonstrate that prebiotic molecules could be synthesised on the surface of charged dust grains that are submerged in an atmospheric plasma. In order to assess the potential role of lightning in brown dwarfs and extrasolar planetary atmospheres, we applied laboratory and numerical scaling laws for streamer discharges to atmospheres where mineral clouds form. A comparison between the breakdown electric field and the local electric field shows that electrical breakdown can occur at two locations: inside the cloud layer (intra-cloud lightning) and above the cloud layer (sprite). Boccippio et al. (1995) observed that 80% of the sprites on Earth coincide with lightning ground strokes which was confirmed by numerical modelling in combination with high-speed measurements of sprite optical emissions (Liu et al. 2009; Gameraota et al. 2011).

From these locations in the atmosphere, the discharge propagates through the atmosphere with subsequent branching until a minimum diameter is reached and the discharge terminates. The total length of the lightning strike generally extends over a longer distance in the atmosphere of a brown dwarf than of a giant gas planet. Consequently, the atmospheric gas volume affected by one of these discharge events (e.g. by an increase of heat or an increase of the local number of electrons) is larger in a brown dwarf atmosphere ( $10^8 - 10^{10} \text{ m}^3$ ) than in a giant gas planet’s atmosphere ( $10^4 - 10^6 \text{ m}^3$ ). The total dissipated energy in one event is  $< 10^{12} \text{ J}$  for all models of initial solar metallicity which is below the values observed for Saturn and Jupiter. The dissipated energy is higher in brown dwarf atmospheres than in giant gas planetary atmospheres and increases with decreasing effective temperature in both cases.

This all suggests that lightning events occurring in the atmospheres of BDs may be easier

---

2012). Krasnopolsky (2006) suggested that the observed NO abundance in Venus’s atmosphere may be the result of lightning discharges. On Earth, they typically emit in the blue and red range of the spectrum. Borucki et al. (1996) simulated the atmosphere of a Jupiter-like planet and found that the He 588 nm line could appear in the spectrum of a lightning discharge. Tessenyi et al. (2013) found that ozone’s 9.6 and 14.3  $\mu\text{m}$  band could be significant in the atmosphere of super-Earths.

to observe than on planets. However, the likelihood of detection depends on the energetics of the discharge and the proximity of its host to Earth. Many of the known exoplanets, in particular those in the habitable zone, are considerably farther away from Earth than the nearest brown dwarfs (e.g. Lo Curto et al. 2013). Therefore, a non-detection is not evidence for the absence of lightning on exoplanets.

The energy release by lightning is dissipated into the ambient medium and, hence, causes an increase of the gas temperature inside the discharge channel. Assuming that the chemistry remains in a steady state (for all kinetic reactions  $\tau_{\text{chem}} < 10^{-4}\text{s}$ ), we have presented a tentative investigation of the impact lightning has on the molecular composition of a GP atmospheric gas of solar metallicity. We modelled the enhanced temperature in a localised atmospheric volume as a result of the discharge event, and its effect on the local chemistry. First attempts to show the influence of lightning on the local gas phase indicate an increase of small carbohydrate molecules like CH and CH<sub>2</sub> at the expense of CO and CH<sub>4</sub>. Dust forming molecules are destroyed and the dust properties are frozen-in unless enough time is available for complete evaporation.

The dissipated energy per lightning event calculated from our simplified model is comparable to terrestrial values, and only reach values comparable to Jupiter in a low-metallicity atmosphere which is  $\sim 10^4 - 10^5 \times$  the terrestrial value. As there is no reason to doubt the fundamental physics of streamer propagation being applicable outside of our solar system, external factors like rotation rates and cosmic rays may influence the occurrence of such large-scale discharges. Rimmer & Helling (2013) show that cosmic rays can ionise the upper atmosphere of free-floating brown dwarfs and giant gas planets, and cosmic rays **may** also trigger lightning (Beloglazov & Akhmetov 2010; Rycroft & Harrison 2012; Babich et al. 2012). The impact of cosmic rays will be stronger for a brown dwarf because they are not shielded by a host star’s wind. Brown dwarfs can be rapid rotators (e.g. Scholz et al. 2011) which influences the wind speeds and the local conditions for charge separation. Volcano plumes, which are composed of small silicate ash particles, have a lightning activity that is order of magnitudes larger than in a common thundercloud on Earth. These arguments suggest that our results provide a lower limit for the lightning dissipation energy and that lightning can be expected to be stronger and more frequent in fast rotating extraterrestrial objects that form mineral clouds.

**Acknowledgement:** We thank the anonymous referee for a very constructive refereeing process. We thank Declan A. Diver, M. Füllekrug, Aline Vidotto, Scott Gregory, and Peter Voitke for helpful discussions. ChH, CRS, GH highlight financial support of the European Community under the FP7 by an ERC starting grant. RB thanks the Physics Trust of the University of St Andrews for supporting her summer placement. Most literature search was

performed using the ADS. Our local computer support is highly acknowledged.

## REFERENCES

- Akalin, F., Gurnett, D. A., Averkamp, T. F., et al. 2006, *Geophys. Res. Lett.*, 33, 20107
- Aplin, K. L. 2013, *Electrifying Atmospheres: Charging, Ionisation and Lightning in the Solar System and Beyond*, doi:10.1007/978-94-007-6633-4
- Babich, L. P., Bochkov, E. I., Dwyer, J. R., & Kutsyk, I. M. 2012, *Journal of Geophysical Research (Space Physics)*, 117, 9316
- Beloglazov, M. I., & Akhmetov, O. I. 2010, *Geomagnetism and Aeronomy/Geomagnetizm i Aeronomiia*, 50, 781
- Belu, A. R., Selsis, F., Raymond, S. N., et al. 2013, *ApJ*, 768, 125
- Berger, E., Basri, G., Fleming, T. A., et al. 2010, *ApJ*, 709, 332
- Boccippio, D. J., Williams, E. R., Heckman, S. J., et al. 1995, *Science*, 269, 1088
- Borovsky, J. E. 1995, *J. Geophys. Res.*, 100, 2697
- Borucki, W. J., McKay, C. P., Jebens, D., Lakkaraju, H. S., & Vanajakshi, C. T. 1996, *Icarus*, 123, 336
- Braude, S. I., Megn, A. V., Riabov, B. P., Sharykin, N. K., & Zhuk, I. N. 1978, *Ap&SS*, 54, 3
- Briels, T. M. P., Kos, J., van Veldhuizen, E. M., & Ebert, U. 2006, *Journal of Physics D Applied Physics*, 39, 5201
- Briels, T. M. P., Kos, J., Winands, G. J. J., van Veldhuizen, E. M., & Ebert, U. 2008a, *Journal of Physics D Applied Physics*, 41, 234004
- Briels, T. M. P., van Veldhuizen, E. M., & Ebert, U. 2008b, *Journal of Physics D Applied Physics*, 41, 234008
- Burgasser, A. J., Melis, C., Zauderer, B. A., & Berger, E. 2013, *ApJ*, 762, L3
- Burgasser, A. J., Sitarski, B. N., Gelino, C. R., Logsdon, S. E., & Perrin, M. D. 2011, *ApJ*, 739, 49

- Cook, B. A., Williams, P. K. G., & Berger, E. 2013, ArXiv e-prints, arXiv:1310.6758
- Cooray, V. 1997, *J. Geophys. Res.*, 102, 21401
- Cummer, S. A., Jaugey, N., Li, J., et al. 2006, *Geophysical Research Letters*, 33, 4104
- Dehn, M. 2007, PhD Thesis, University Hamburg
- Desch, M. D. 1992, in *Planetary Radio Emissions III*, Proceedings of the 3rd International Workshop held at Graz, Austria, September 2-4, 1991. Edited by H.O. Rucker, S.J. Bauer, and M.L. Kaiser. Austrian Academy of Sciences Press, Vienna, 1985., p.371, ed. H. O. Rucker, S. J. Bauer, & M. L. Kaiser, 371
- Desch, S. J., Borucki, W. J., Russell, C. T., & Bar-Nun, A. 2002, *Reports on Progress in Physics*, 65, 955
- Dickinson, J. T., Jensen, L. C., & Jahan-Latibari, A. 1984, *Journal of Vacuum Science Technology*, 2, 1112
- Dobbs-Dixon, I., Agol, E., & Burrows, A. 2012, *ApJ*, 751, 87
- Dubrovin, D., Nijdam, S., van Veldhuizen, E. M., et al. 2010, *Journal of Geophysical Research (Space Physics)*, 115, 0
- Dwyer, J. R., Smith, D. M., & Cummer, S. A. 2012, *Space Sci. Rev.*, 173, 133
- Dwyer, J. R., Rassoul, H. K., Al-Dayeh, M., et al. 2004, *Geophys. Res. Lett.*, 31, 5118
- Dyudina, U. A., del Genio, A. D., Ingersoll, A. P., et al. 2004, *Icarus*, 172, 24
- Ebert, U., Nijdam, S., Li, C., et al. 2010a, *Journal of Geophysical Research (Space Physics)*, 115, 0
- . 2010b, *Journal of Geophysical Research (Space Physics)*, 115, 0
- Ehrenreich, D., Tinetti, G., Lecavelier Des Etangs, A., Vidal-Madjar, A., & Selsis, F. 2006, *A&A*, 448, 379
- Farrell, W. M., Kaiser, M. L., & Desch, M. D. 1999, *Geophys. Res. Lett.*, 26, 2601
- Fischer, G., Gurnett, D. A., Kurth, W. S., et al. 2008, *Space Sci. Rev.*, 137, 271
- Fischer, G., Kurth, W. S., Gurnett, D. A., et al. 2011, *Nature*, 475, 75
- Füllekrug, M., Kolmasova, I., Santolik, O., et al. 2013, 0

- Gamerota, W. R., Cummer, S. A., Li, J., et al. 2011, *Journal of Geophysical Research (Space Physics)*, 116, 2317
- Gerken, E. A., Inan, U. S., & Barrington-Leigh, C. P. 2000, *Geophysical Research Letters*, 27, 2637
- Gillon, M., Triaud, A. H. M. J., Jehin, E., et al. 2013, *ArXiv e-prints*, arXiv:1304.0481
- Green, J. C., Froning, C. S., Osterman, S., et al. 2012, *ApJ*, 744, 60
- Gurnett, D. A., Kurth, W. S., Cairns, I. H., & Granroth, L. J. 1990, *J. Geophys. Res.*, 95, 20967
- Hall, P. B. 2002, *ApJ*, 580, L77
- Harland, W. B., & Haker, J. 1966, *Adv.Sci.*, 22, 663
- Helling, C., Dehn, M., Woitke, P., & Hauschildt, P. H. 2008a, *Astrophysical Journal*, 675, L105
- . 2008b, *Astrophysical Journal*, 677, L157
- Helling, C., Jardine, M., Diver, D., & Stark, C. 2013, (*ApJ*), 767, 136
- Helling, C., Jardine, M., & Mokler, F. 2011a, *ApJ*, 737, 38
- Helling, C., Jardine, M., Witte, S., & Diver, D. A. 2011b, *Astrophysical Journal*, 727, 4
- Helling, C., Ackerman, A., Allard, F., et al. 2008c, *MNRAS*, 391, 1854
- Heng, K., Menou, K., & Phillipps, P. J. 2011, *MNRAS*, 413, 2380
- Hernandez, S., & et al. 2012, *Space Telescope Imaging Spectrograph Instrument Handbook for Cycle 21 v. 12.0*
- Houck, J. R., Roellig, T. L., van Cleve, J., et al. 2004, *ApJS*, 154, 18
- Hurley, J., Irwin, P. G. J., Fletcher, L. N., et al. 2012, *Planet. Space Sci.*, 65, 21
- Johnson, A. P., Cleaves, H. J., Dworkin, J. P., et al. 2008, *Science*, 322, 404
- Kassim, N. E., Polisensky, E. J., Clarke, T. E., et al. 2005, in *Astronomical Society of the Pacific Conference Series*, Vol. 345, *From Clark Lake to the Long Wavelength Array: Bill Erickson’s Radio Science*, ed. N. Kassim, M. Perez, W. Junor, & P. Henning, 392

- Käuffl, H.-U., Ballester, P., Biereichel, P., et al. 2004, in Society of Photo-Optical Instrumentation Engineers (SPIE) Conference Series, Vol. 5492, Ground-based Instrumentation for Astronomy, ed. A. F. M. Moorwood & M. Iye, 1218–1227
- Knutson, H. A., Lewis, N., Fortney, J. J., et al. 2012, *ApJ*, 754, 22
- Kovács, T., & Turányi, T. 2010, *Icarus*, 207, 938
- Krasnopolsky, V. A. 2006, *Icarus*, 182, 80
- Krider, E. P., Dawson, G. A., & Uman, M. A. 1968, *J. Geophys. Res.*, 73, 3335
- Kumar, A., Ghosh, S. K., Hutchings, J., et al. 2012, in Society of Photo-Optical Instrumentation Engineers (SPIE) Conference Series, Vol. 8443, Society of Photo-Optical Instrumentation Engineers (SPIE) Conference Series
- Lacy, J. H., Richter, M. J., Greathouse, T. K., Jaffe, D. T., & Zhu, Q. 2002, *PASP*, 114, 153
- Le Fèvre, O., Saisse, M., Mancini, D., et al. 2003, in Society of Photo-Optical Instrumentation Engineers (SPIE) Conference Series, Vol. 4841, Instrument Design and Performance for Optical/Infrared Ground-based Telescopes, ed. M. Iye & A. F. M. Moorwood, 1670–1681
- Little, B., Anger, C. D., Ingersoll, A. P., et al. 1999, *Icarus*, 142, 306
- Liu, N., & Pasko, V. P. 2007, *Geophys. Res. Lett.*, 34, 16103
- Liu, N. Y., Pasko, V. P., Adams, K., Stenbaek-Nielsen, H. C., & McHarg, M. G. 2009, *Journal of Geophysical Research (Space Physics)*, 114, 0
- Lo Curto, G., Mayor, M., Benz, W., et al. 2013, *ArXiv e-prints*, arXiv:1301.2741
- Lorenz, R. D. 2008, *Space Sci. Rev.*, 137, 295
- Lu, G., Cummer, S. A., Li, J., et al. 2011, *Journal of Geophysical Research (Space Physics)*, 116, 3316
- MacGorman, D., & Rust, W. 1998, *The electric nature of storms* (Oxford University Press)
- MacLachlan, C. S., Potts, H. E., & Diver, D. A. 2013, *Plasma Sources Science Technology*, 22, 015025
- Mandell, A. M., Bast, J., van Dishoeck, E. F., et al. 2012, *ApJ*, 747, 92
- Marisaldi, M., Tavani, M., Argan, A., et al. 2010, *AGU Fall Meeting Abstracts*, A330

- Mayor, M., Pepe, F., Queloz, D., et al. 2003, *The Messenger*, 114, 20
- McHarg, M. G., Stenbaek-Nielsen, H. C., Kanmae, T., & Haaland, R. K. 2010, *Journal of Geophysical Research (Space Physics)*, 115, 0
- McLean, I. S., Becklin, E. E., Bendiksen, O., et al. 1998, in *Society of Photo-Optical Instrumentation Engineers (SPIE) Conference Series*, Vol. 3354, *Infrared Astronomical Instrumentation*, ed. A. M. Fowler, 566–578
- Meegan, C., Lichti, G., Bhat, P. N., et al. 2009, *ApJ*, 702, 791
- Merrison, J. P., Gunnlaugsson, H. P., Hogg, M. R., et al. 2012, *Planet. Space Sci.*, 60, 328
- Miller, S., & Urey, H. 1953, *Science*, 117
- Miller, S. L., & Urey, H. C. 1959, *Science*, 130, 245
- Nichols, J. D., Burleigh, M. R., Casewell, S. L., et al. 2012, *ApJ*, 760, 59
- Nijdam, S., Moerman, J. S., Briels, T. M. P., van Veldhuizen, E. M., & Ebert, U. 2008, *Applied Physics Letters*, 92, 101502
- Noxon, J. F. 1976, *Geophys. Res. Lett.*, 3, 463
- Pancheshnyi, S., Nudnova, M., & Starikovskii, A. 2005, *Physical Review E*, 71, 016407
- Pasko, V. P. 2007, *Plasma Sources Science Technology*, 16, 13
- Pasko, V. P., Inan, U. S., & Bell, T. F. 2000, *Geophys. Res. Lett.*, 27, 497
- Pasko, V. P., Inan, U. S., Bell, T. F., & Taranenko, Y. N. 1997, *Journal of Geophysical Research*, 102, 4529
- Paxton, A. H., Gardner, R. L., & Baker, L. 1986, *Physics of Fluids*, 29, 2736
- Perna, R., Heng, K., & Pont, F. 2012, *ApJ*, 751, 59
- Phelps, C. T. 1974, *Journal of Atmospheric and Terrestrial Physics*, 36, 103
- Raizer, Y. 1991, *Gas Discharge Physics* (Berlin, Springer)
- Raizer, Y. P., Milikh, G. M., Shneider, M. N., & Novakovski, S. V. 1998, *Journal of Physics D Applied Physics*, 31, 3255
- Rakov, V., & Uman, M. 2003, *Lightning: Physics and Effects* (Cambridge University Press)

- Rauscher, E., & Menou, K. 2012, *ApJ*, 750, 96
- Rimmer, P., & Helling, C. 2013, (*ApJ*, submitted), 0, 0
- Rinnert, K., Lanzerotti, L. J., Uman, M. A., et al. 1998, *Journal of Geophysical Research*, 103, 22979
- Roming, P. W. A., Kennedy, T. E., Mason, K. O., et al. 2005, *Space Sci. Rev.*, 120, 95
- Roussel-Dupré, R., Colman, J. J., Symalisky, E., Sentman, D., & Pasko, V. P. 2008, *Space Science Reviews*, 137, 51
- Route, M., & Wolszczan, A. 2013, *ApJ*, 773, 18
- Rycroft, M., & Harrison, R. 2012, *Space Science Review*, 168, 363
- Scholz, A., Irwin, J., Bouvier, J., et al. 2011, *MNRAS*, 413, 2595
- Showman, A. P., Fortney, J. J., Lewis, N. K., & Shabram, M. 2013a, *ApJ*, 762, 24
- . 2013b, *ApJ*, 762, 24
- Stark, C. R., Helling, C., Diver, D. A., & Rimmer, P. B. 2013, *ArXiv e-prints*, arXiv:1311.4408
- Stenbaek-Nielsen, H. C., McHarg, M. G., Kanmae, T., & Sentman, D. D. 2007, *Geophysical Research Letters*, 34, 11105
- Tavani, M., Barbiellini, G., Argan, A., et al. 2006, in *Society of Photo-Optical Instrumentation Engineers (SPIE) Conference Series*, Vol. 6266, *Society of Photo-Optical Instrumentation Engineers (SPIE) Conference Series*
- Tessenyi, M., Tinetti, G., Savini, G., & Pascale, E. 2013, *Icarus*, 226, 1654
- van Haarlem, M. P., Wise, M. W., Gunst, A. W., et al. 2013, *A&A*, 556, A2
- Vernet, J., Dekker, H., D’Odorico, S., et al. 2011, *A&A*, 536, A105
- Viana, A. 2009, *Near Infrared Camera and Multi-Object Spectrometer Instrument Handbook for Cycle 17 v. 11.0*
- Wallace, L. 1964, *ApJ*, 139, 994
- Williams, P. K. G., Berger, E., & Zauderer, B. A. 2013a, *ApJ*, 767, L30

- Williams, P. K. G., Cook, B. A., & Berger, E. 2013b, ArXiv e-prints, arXiv:1310.6757
- Witte, S., Helling, C., Barman, T., Heidrich, N., & Hauschildt, P. H. 2011, A&A, 529, A44
- Witte, S., Helling, C., & Hauschildt, P. H. 2009, Astronomy and Astrophysics, 506, 1367
- Woitke, P., & Helling, C. 2004, A&A, 414, 335
- Woitke, P., Krueger, D., & Sedlmayr, E. 1996, A&A, 311, 927
- Yair, Y. 2012, Advances in Space Research, 50, 293
- Yair, Y., Fischer, G., Simões, F., Renno, N., & Zarka, P. 2008, Space Sci. Rev., 137, 29
- Yair, Y., Takahashi, Y., Yaniv, R., Ebert, U., & Goto, Y. 2009, Journal of Geophysical Research (Planets), 114, 9002
- Zarka, P., Farrell, W. M., Fischer, G., , & Konovalenko, A. 2008, in Planetary Atmospheric Electricity, Edited by F. Leblanc, K.L. Aplin, Y. Yair, R.G. Harrison. J.P. Lebreton, M. Blanc, p.257, ed. F. Leblanc, K. L. Aplin, Y. Yari, R. G. Harrison, L. J. P., & B. M., 257
- Zarka, P., Farrell, W. M., Kaiser, M. L., Blanc, E., & Kurth, W. S. 2004, Planet. Space Sci., 52, 1435
- Zarka, P., & Pedersen, B. M. 1986, Nature, 323, 605
- Zarka, P., Bougeret, J.-L., Briand, C., et al. 2012, Planet. Space Sci., 74, 156

Process	Signature	Wavelength	Celestial body	References	Instrument with suitable wavelength range
Direct lightning emission	$\gamma$ - ray (TGF)	20 eV - 40 MeV	Earth	Lu et al. (2011); Yair (2012) Marisaldi et al. (2010)	Fermi GBM, Meegan et al. (2009) AGILE, Tavani et al. (2006)
	X - ray	30 – 250 keV		Dwyer et al. (2004) Dwyer et al. (2012)	AGILE Astrosat-SXT <sup>1</sup> Astrosat-LAXPC <sup>2</sup>
	He	588 nm	Jupiter	Borucki et al. 1996 Aplin (2013)	VLT - X-SHOOTER Vernet et al. (2011) VLT - VIMOS, Le Fèvre et al. (2003)
	NUV to NIR many lines of N <sub>2</sub> , N(II), O(I), O(II)	See: Wallace (1964) (310-980 nm) 0.35-0.85 $\mu$ m (direct imaging)	Earth Jupiter	Wallace (1964) Baines et al. 2007	Astrosat - UVIT, Kumar et al. (2012) Swift-UVOT, Roming et al. (2005) VLT - X-SHOOTER VLT - VIMOS HARPS, Mayor et al. (2003) HST-NICMOS, Viana (2009) IRTF - TEXES, Lacy et al. (2002) Spitzer IRS, Houck et al. (2004)
	whistlers	tens of Hz - kHz	Earth Saturn Jupiter	Desch et al. (2002) Yair et al. (2008); Yair (2012) Akalin et al. (2006) Fischer et al. (2008)	LOFAR, van Haarlem et al. (2013) UTR 2, Braude et al. (1978) LWA, Kassim et al. (2005)
	sferics	1 kHz - 100 MHz	Earth Saturn Uranus	Desch et al. (2002) Yair et al. (2008) Fischer et al. (2008) Zarka & Pedersen (1986)	LOFAR UTR 2 LWA
Effect on local chemistry	NO <sub>x</sub>	439 nm (NO <sub>2</sub> ) 445 nm (NO <sub>2</sub> ) 5.3 $\mu$ m (NO)	Earth Venus	Lorenz (2008) Noxon (1976) Krasnopolsky (2006)	HST-STIS Hernandez & et al. (2012) VLT -X-SHOOTER VLT - VIMOS
	O <sub>3</sub>	9.6 $\mu$ m 14.3 $\mu$ m 200 – 350 nm 420 – 830 nm	Earth	Tessenyi et al. (2013)  Ehrenreich et al. (2006)	HARPS HST - NICMOS IRTF-TEXES Spitzer IRS
	HCN	2.97525 $\mu$ m 3.00155 $\mu$ m	Jupiter	Desch et al. (2002)	VLT - CRIRES, Käufel et al. (2004)
	C <sub>2</sub> H <sub>2</sub>	2.998 $\mu$ m 3.0137 $\mu$ m		Mandell et al. (2012)	Keck - NIRSPEC, McLean et al. (1998)
Emission caused by secondary events (e.g. sprites) <sup>3</sup>	1PN <sub>2</sub>	609 – 753 nm	Earth	Pasko (2007) Liu & Pasko (2007)	HST - STIS VLT - X-SHOOTER VLT - VIMOS
	1NN <sub>2</sub> <sup>+</sup>	391.4 nm			HARPS
	2PN <sub>2</sub>	337 nm			HST-COS, Green et al. (2012) HST-STIS
	LBH N <sub>2</sub>	150 – 280 nm			

<sup>1</sup> <http://astrosat.iucaa.in/?q=node/14>

<sup>2</sup> <http://astrosat.iucaa.in/?q=node/12>

<sup>3</sup> 1PN<sub>2</sub> is the first, 2PN<sub>2</sub> is the second positive, LBH N<sub>2</sub> is the Lyman-Birge-Hopfield N<sub>2</sub> band system. 1NN<sub>2</sub><sup>+</sup> is the first negative band system of N<sub>2</sub><sup>+</sup>.

Table 1: Lightning discharges signatures observed in the Solar System. The right column lists potentially useful instruments to observe lightning on extrasolar planets or brown dwarfs.